AGU PUBLICATIONS

Water Resources Research

RESEARCH ARTICLE

10.1002/2013WR014631

Electrical-hydraulic relationships observed for unconsolidated sediments in the presence of a cobble framework

Lee Slater[1], Warren Barrash[2], Jeanette Montrey[1], and Andrew Binley[3]

[1]Department of Earth and Environmental Sciences, Rutgers-Newark, Newark, New Jersey, USA, [2]Center for Geophysical Investigation of the Shallow Subsurface, Department of Geosciences, Boise State University, Boise, Idaho, USA, [3]Lancaster Environment Centre, Lancaster University, Lancaster, UK

Key Points:
- The cobble framework complicates interpretation of *K* from SIP
- Discounting the cobble framework improves SIP estimation of *K*
- Such discounting also improves estimation of imaginary conductivity

Correspondence to:
L. Slater,
lslater@rutgers.edu

Citation:
Slater, L., W. Barrash, J. Montrey, and A. Binley (2014), Electrical-hydraulic relationships observed for unconsolidated sediments in the presence of a cobble framework, *Water Resour. Res.*, *50*, 5721–5742, doi:10.1002/2013WR014631.

Received 22 AUG 2013
Accepted 24 JUN 2014
Accepted article online 26 JUN 2014
Published online 12 JUL 2014

Abstract Mechanistic models now exist to predict hydraulic conductivity (*K*) from the spectral-induced polarization (SIP) response of granular media. We examined the predictions of such a model on unconsolidated coarse fluvial sediments and compared them to those obtained with a modified Kozeny-Carman (KC) model. Samples were retrieved from the Boise Hydrogeophysical Research Site (BHRS), located on a gravel bar adjacent to the Boise River, Idaho. A sample holder (0.102 m diameter and 0.12 m in length) was designed to include the cobble framework in reconstituted samples representing the primary stratigraphic units defined based on porosity variation at this site. SIP (0.001–1000 Hz) and *K* (from Darcy tests) measurements were recorded for 12 samples, with SIP measurements made as a function of pore fluid conductivity (3–300 mS/m), grain size distribution (GSD), and total porosity. *K* prediction with the KC model was improved after discounting of the cobble framework and multiplying by the tortuosity resulting from matrix "capillaries" around the cobbles, resulting in estimates within a factor of 5 of the measurements. *K* prediction with a mechanistic SIP model based on Stern layer polarization (SLP model) that requires an estimate of the GSD also required discounting for the cobble framework to obtain estimates within 0.5 orders of magnitude of the measurements. Similarly, the SLP model overpredicts the measured imaginary conductivity (σ'') unless the cobble framework is discounted, which then results in estimates of σ'' within a factor of 2 of the measurements. This can be explained by the fact that the cobbles polarize at frequencies well below the minimum measurement frequency (0.001 Hz). The SLP model for *K* prediction parameterized in terms of the formation factor and imaginary conductivity performed well for the 10 samples with a cobble framework without modification as the imaginary conductivity directly senses the matrix grain size characteristics, whereas the formation factor captures the porosity reduction and tortuosity resulting from the presence of the cobble framework (capillary tortuosity). Our findings suggest that the estimation of contrasts in *K* in coarse sediments may be achievable through measurements of electrical properties after appropriate consideration of the cobble fraction.

1. Introduction

The sensitivity of electrical geophysical measurements to the hydraulic properties of porous soils and sediments has long motivated efforts to estimate hydraulic conductivity (*K*) from electrical properties. One common approach starts with the bundle of capillaries model that is defined by the Kozeny-Carman (KC) equation [*Kozeny*, 1927; *Carman*, 1937] and recognizes an improvement to this model that can result from substituting the porosity ($\varnothing$) with the electrical formation factor (*F*) that is sensitive to both the volume and connectivity of the pore space [*Revil and Cathles*, 1999]. The development of the induced polarization (IP) method has accelerated efforts to estimate *K* from electrical measurements in recent years [see *Revil and Flosch*, 2010; *Revil*, 2012]. Such efforts have been motivated by the fact that the IP method senses additional parameters describing the polarization of the electrical double layer at the mineral-fluid interface and that are also relevant to *K* estimation (grain size, pore size, and specific surface area) [*Börner and Schön*, 1991; *Sturrock*, 1999; *Lesmes and Morgan*, 2001; *Titov et al*., 2002; *Scott and Barker*, 2003, 2005; *Binley et al*., 2005; *Kemna et al*., 2005; *Tong et al*., 2006a, 2006b; *Leroy et al*., 2008]. The interfacial surface area per unit pore volume (S_{por}) is an often accepted measurable property representing the inverse of the hydraulic radius appearing in the KC equation [e.g., *Charbeneau*, 2000]. Furthermore, when spectral IP measurements are made over a range of frequencies, it becomes possible to estimate the length scale (or a distribution of length scales) of the polarization processes. Recent studies suggested that this length scale may be closely

associated with the length scale determining flow in porous media, offering addition opportunities for the estimation of hydraulic conductivity from electrical geophysical measurements [*Binley et al*., 2005; *Revil and Florsch*, 2010; *Zisser et al*., 2010; *Revil*, 2012].

Most of these efforts have examined either sandstone samples or reconstituted unconsolidated sand to clay size sediments. High-energy, unconsolidated fluvial and periglacial depositional systems may contain a cobble-dominated framework that demands a correction to KC-type *K* estimates whereby the contribution of the cobble framework must be discounted as it does not contribute to the fluid flow [*Clarke*, 1979; *Jussel et al*., 1994; *Koltermann and Gorelick*, 1995]. How the presence of a cobble framework would modify the performance of recently proposed electrical models for *K* estimation from IP measurements has not been investigated.

In this study, we describe a set of electrical and hydraulic measurements performed on unconsolidated coarse fluvial sediments characterized by a cobble framework known to influence the estimation of *K* from grain size-based KC formulations. Such sediments are widespread in high-energy fluvial, periglacial, and semiarid tectonically active environments—and appropriate approaches to estimating and measuring *K* in these deposits are an active area of research [e.g., *Jussel et al*., 1994; *Klingbeil et al*., 1999; *Heinz et al*., 2003; *Lunt et al*., 2004; *Barrash and Cardiff*, 2013; *Cardiff et al*., 2013]. In this regard, while the KC model is not ideally suited for sediments with wide ranges in grain size distribution or cobble framework structure, extensive experience with this model and appropriate modifications for nonuniform sediments [e.g., *Bear*, 1972; *Freeze and Cherry*, 1979; *Panda and Lake*, 1994] including cobble framework sediments or functional equivalents [e.g., *Clarke*, 1979; *Jussel et al*., 1994; *Koltermann and Gorelick*, 1995; *Klingbeil et al*., 1999; *Heinz et al*., 2003; *Hu et al*., 2009] provides the basis for using and modifying the KC model here for comparison with both previous similar applications and electrical models. That is, we do not advocate the use of the KC model for such sediments, but we do find merit in the use of the model as a baseline against which to compare the performance of novel electrical models for *K* estimation, being the focus of this study.

We test the effectiveness of the recently developed grain size polarization-based model for *K* estimation presented in *Revil and Florsch* [2010] and compare it to KC estimates. We henceforth term the *Revil and Florsch* [2010] model the Stern Layer Polarization (SLP) model as it is built on the assumption that the Stern layer around soil particles is discontinuous and thus polarizable. Just as with KC model, we find it is necessary to discount the cobble framework to predict *K* when using the SLP model formulated in terms of the grain size distribution (GSD). The formation factor, usually a measure of the effective porosity of the interconnected pores, is strongly controlled by the cobble framework. The imaginary component of the electrical conductivity (σ'') that quantifies the polarization of the interfacial surface is insensitive to the cobble framework, requiring the discounting of the cobbles to reliably estimate σ'' from the GSD. However, as σ'' is directly sensitive to the matrix GSD, the SLP model works well on these cobble samples when it is directly parameterized in terms of *F* and σ''.

2. Petrophysical Models

2.1. Hydraulic Conductivity (K)

KC-type equations are frequently used to estimate *K* from measurements of total porosity ($\varnothing$) and either specific surface area or parameters describing the GSD. For example, *Bear* [1972] presents the following equation for KC-derived *K* (K_{KC}):

$$K_{KC} = \frac{\rho_w g}{\mu} \frac{\varnothing^3 d_{10}^2}{180(1-\varnothing^2)}, \tag{1}$$

where d_{10} represents the grain size at which 10% of the sample is finer by weight, ρ_w is fluid density, *g* is the gravitational acceleration, and μ is the dynamic viscosity. As previously mentioned, KC models must be modified to account for a cobble "framework." *Hu et al*. [2009] present such a modification, based on an assumption that, for a sedimentary unit consisting of sands and gravels with significant cobbles (e.g., bimodal GSD), groundwater flow will occur through the "matrix" of sands and fine gravels existing within the interstices of the cobble framework [e.g., *Clarke*, 1979; *Koltermann and Gorelick*, 1995] (Figure 1). The size break between matrix and framework cobbles has been recognized to be about 0.01 m at the BHRS and numerous other sites with similar sediments [*Smith*, 1986; *Todd*, 1989; *Shih and Komar*, 1990; *Jussel et al*., 1994; *Barrash and Reboulet*, 2004]. Identifying the framework cobble (V_c) and matrix (V_m) volume fractions of the total sample volume, $\varnothing + V_c + V_m = 1$, and the framework cobbles represent a fraction of the flow

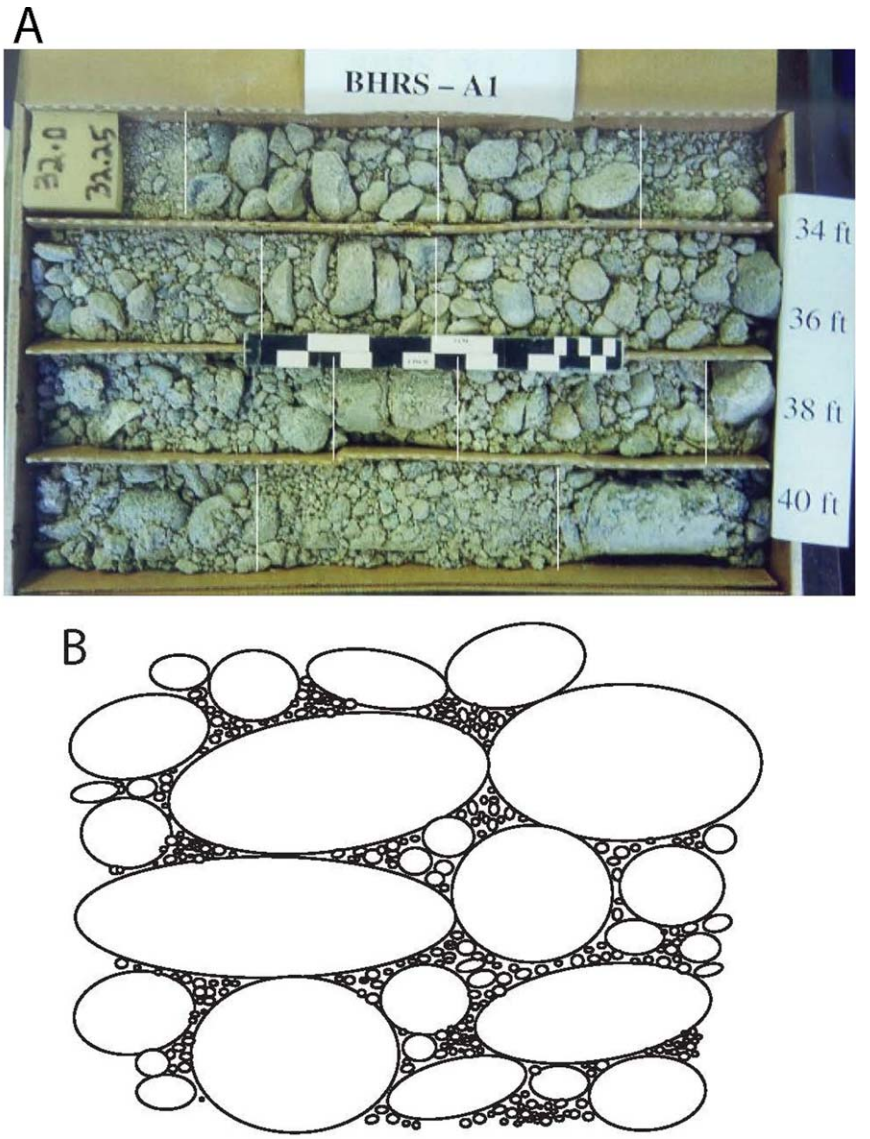

Figure 1. (a) Example of core collected in well A1 with lines showing boundaries between sample subdivisions based on cobble size and proportion and matrix composition. (b) Cartoon sketch of cross-section through cobble framework and matrix; in such a medium, groundwater flows in the matrix porosity and takes tortuous paths around the framework cobbles.

cross-section (equal to the dominant fraction of the sample volume) blocking flow. The sample porosity used in the modified KC equation is then adjusted to be totally assigned to the matrix, $\varnothing_m = \varnothing/(\varnothing + V_m)$, in order to determine a hydraulic conductivity representing the matrix portion of the aquifer (K_m)

$$K_m = \frac{\rho_w g}{\mu} \frac{\varnothing_m^3 d_{10[m]}^2}{180(1-\varnothing_m)^2}, \tag{2}$$

where $d_{10[m]}$ is the grain size at which 10% of the matrix fraction is finer by weight. The hydraulic conductivity estimate of the whole sample is then computed from

$$K_{KC[mod]} = K_m(\varnothing + V_m). \tag{3}$$

Here we note that d_{10} and $d_{10[m]}$ are used in equations (1) and (2) as example effective or representative grain sizes for the whole GSD or the GSD of the matrix fraction of coarse conglomeratic sediments with cobble framework. Indeed it has been recognized by many that no single grain size has proven to be the

representative or effective grain size for all aquifers or aquifer materials in the KC sense, and so the d value in the KC equation is an effective diameter or representative diameter for a given site-specific or material-specific aquifer or aquifer material [e.g., *Bear*, 1972; *Freeze and Cherry*, 1979; *Domenico and Schwartz*, 1990; *Charbeneau*, 2000, and many others]. In this paper, as we examine hydraulic and electrical behavior, we use several specific grain sizes that are commonly used for both the GSD as a whole and the matrix fraction (e.g., d_{10}, d_{50}, and d_{60}), and we explain why a given grain size is used in different cases. Also, we use the term "true effective grain size" to acknowledge that an aquifer-specific or sample-specific grain size could be a better fit for a given constitutive equation rather than a generalized value like d_{10}, d_{50}, or d_{60}.

2.2. Complex Conductivity

The measured complex electrical conductivity is given by $\sigma^* = \sigma' + i\sigma''$, where the real ($\sigma'$) and imaginary ($\sigma''$) components represent the ohmic conduction and polarization charge transport mechanisms in a porous medium, respectively. The measured phase shift is related to the real and imaginary parts of the complex conductivity according to $tan^{-1}\left(\sigma'/\sigma''\right)$, and the measured conductivity magnitude is given by $|\sigma| = \sqrt{(\sigma')^2 + (\sigma'')^2}$.

Most models for the complex electrical conductivity of a porous material at low frequencies (e.g., less than 100 Hz) include a parallel addition of two conduction mechanisms representing (1) an electrolytic contribution via conduction through the interconnected pore space (σ_{el}), and (2) a mineral surface contribution via conduction within the electrical double layer (EDL) forming at the interfaces of the interconnected pore surface (σ_s^*) [e.g., *Vinegar and Waxman*, 1984; *Revil*, 2012], such that $\sigma^* = \sigma_{el} + \sigma_s^*$. As the electrolyte is essentially unpolarizable at low frequencies, electrolytic conduction is a purely real term. In contrast, the surface conductivity has contributions from both conduction and polarization of ions in the EDL. As $\sigma_{el} = (1/F)\sigma_w$, the measured real part of complex conductivity is given by

$$\sigma' = \frac{1}{F}\sigma_w + \sigma'_s, \tag{4}$$

where F is the electrical formation factor and σ'_s is the real part of the surface conductivity. The measured imaginary part of the complex conductivity is exclusively related to the interfacial polarization, i.e., the imaginary part of the surface conductivity, $\sigma'' = \sigma''_s$.

The complex surface conductivity depends on the physical and chemical properties of the mineral-fluid interface and is frequency-dependent. The SLP model has been extensively described in recent literature [e.g., *Leroy et al*., 2008; *Revil and Florsch*, 2010; *Revil and Skold*, 2011; *Revil*, 2012] and is therefore only briefly reviewed here. This model combines a macroscopic conductivity model for the polarization of a porous medium with a triple layer model for the specific surface conductivity of the Stern layer. Such triple layer models are more sophisticated than the traditional double layer model as they incorporate an inner and outer Stern layer and account for specific adsorption of ions that are tightly bound to the surface in the inner layer (see *Vaudelet et al*. [2011a, 2011b] for more details).

In the SLP model the surface polarization is specifically associated with the Stern layer surrounding the mineral grains, although surface conduction is assumed to occur in both the diffuse and Stern layers [*Revil*, 2012]. The polarization of the Stern layer around a mineral grain is based on a modification of the model of *Schwarz* [1962] for colloidal suspensions. *Leroy et al*. [2008] present the following form of the SLP model:

$$\sigma_s^* = \frac{4}{d_0}\left(\Sigma^d + \Sigma^s\right) - \frac{4}{d_0}\frac{\Sigma^s}{(1 + i\omega\tau_0)}, \tag{5}$$

$$\tau_0 = \frac{d_0^2}{8D}, \tag{6}$$

where d_0 is the mean grain diameter, ω is the angular frequency, Σ^d is the specific surface conductivity associated with the diffuse layer, Σ^s is the specific surface conductivity of the Stern layer, τ_0 is the mean time constant of the relaxation, and D is the diffusion coefficient of the ions in the Stern layer. *Boleve et al*. [2007] conducted experiments on glass beads over the range of salinities from 10^{-4} to 10^{-1} S/m and found $\Sigma^s = 4 \times 10^{-9}$ S as representative for this salinity range.

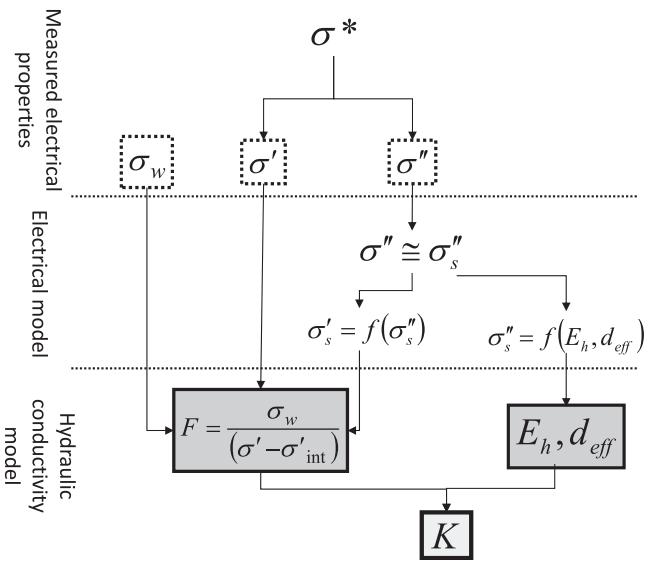

Figure 2. Summary of the link between electrical measurements, electrical properties, and hydraulic properties assumed for *K* estimation from complex conductivity (modified from *Slater* [2007]).

2.3. Relations Between K and Complex Conductivity

Empirical and mechanistic models have been developed in an attempt to predict *K* from electrical measurements [*Börner et al*., 1996; *Slater and Lesmes*, 2002, *Revil and Florsch*, 2010]. The general framework of such models is summarized in the flow chart shown in Figure 2. The imaginary part of the complex conductivity is used as a proxy of surface area or effective grain size, whereas the real part of the complex conductivity, after correction for the influence of surface conduction and in conjunction with a salinity estimate, is used as a proxy of porosity. It is well recognized that *F* can be used to replace the porosity in KC-type formulations to result in better estimates of *K* [*Revil and Cathles*, 1999]. This improvement results from the fact that *F* is sensitive to an effective interconnected porosity ($\varnothing_{eff}$), and it may be assumed that

$$F = \frac{1}{\varnothing_{eff}}, \tag{7}$$

as discussed in *Revil and Cathles* [1999].

The recognized dependence of the complex surface conductivity on surface area and/or the GSD has encouraged efforts to develop *K* predictions from electrical measurements alone [*Börner et al*., 1996; *Revil and Florsch*, 2010]. The SLP model considered here was initially introduced by *Leroy et al*. [2008] and extended by *Revil and Florsch* [2010] with respect to *K* estimation. Our data set includes reasonably accurate estimates of the GSD, including the cobble framework [*Barrash and Reboulet*, 2004] and is well suited for testing the SLP model on coarse materials.

Revil and Florsch [2010] derive two equations for the prediction of *K* based on electrical measurements. The first considered here is a model that uses information on the GSD and *F*

$$K = \frac{\rho_w g}{\mu} \frac{1}{32 m^2 F (F-1)^2} E_h^{-2}, \tag{8}$$

where *m* is the Archie cementation exponent linking the formation factor to the interconnected porosity ($F = \varnothing^{-m}$), and E_h represents the GSD integral

$$E_h = \int_0^{+\infty} f(D) \mathrm{d}\ \ln D, \tag{9}$$

where $f(D)$ is the probability density distribution of the grains of diameter (D) in natural log space. *Revil and Florsch* [2010] show that E_h is equivalent to the expected value of the distribution $h(\eta)$, with $\eta = 1/D$,

$$E_h = \int_0^{+\infty} \eta h(\eta) |d\eta|. \tag{10}$$

Measurements of the full GSD of a material may often be unavailable in field surveys. *Revil and Florsch* [2010] suggested that an average effective grain diameter could be assumed a reasonable approximation of the GSD integral (E_h),

$$\frac{1}{d_{10}} = \xi E_h, \tag{11}$$

where ξ represents a dimensionless normalizing coefficient. *Revil and Florsch* [2010] estimated a value of ξ equal to 32 based on an empirical relationship between imaginary conductivity and d_{10} for a limited set of data for clayey soils reported in *Slater and Lesmes* [2002]. However, d_{10} may not be the best effective grain diameter particularly for coarse grained soils, or even the grain diameter that is well correlated with imaginary conductivity. For example, *Slater and Glaser* [2003] found that the imaginary conductivity grain diameter relationship was strongest for d_{90} for sands/silts from alluvial floodplain deposits. Generally, the value for ξ is not known.

We therefore simplify the relationship by assuming that there will be some effective grain diameter (d_{eff}) that provides the best approximation of the grain size distribution interval such that $\xi \approx 1$, i.e.,

$$\frac{1}{d_{eff}} \approx E_h. \tag{12}$$

Using this approximation equation (8) becomes

$$K \approx \frac{\rho_w g}{\mu} \frac{d_{eff}^2}{32 m^2 F (F-1)^2}. \tag{13}$$

Revil and Florsch [2010] also considered a model to estimate E_h from imaginary conductivity measurements so that a prediction of K based on equation (8) could be made using electrical measurements only. The following relationship between σ'' and the GSD was derived from the SLP model

$$\sigma'' = 4\Sigma^S E_h. \tag{14}$$

Again, in the absence of the full GSD a relationship using an effective grain diameter (d_{eff}) can be defined as

$$\sigma'' = \frac{4\Sigma^S}{\xi d_{10}} \approx \frac{4\Sigma^S}{d_{eff}}. \tag{15}$$

Based on this dependence of σ'' on grain size and assuming m = 1.5 and F >> 1, *Revil and Florsch* [2010] arrive at the following KC-based equation to relate K and σ'':

$$K \approx \frac{\rho_w g}{\mu} \frac{(\Sigma^s)^2}{4.5 F^3} \left(\sigma''\right)^{-2}. \tag{16}$$

Given that a cobble framework must be discounted from Kozeny-Carman estimates of K as it does not contribute to fluid flow, it is intuitive to expect that the cobble framework should not be included in the GSD parameters used in equations (8–15) to estimate K from electrical measurements. We later examine the predictive capability of the Revil and Florsch model described above when the full GSD is included and when the cobble framework is discounted.

3. Study Site: Boise Hydrogeophysical Research Site (BHRS)

To consider the degree to which the above petrophysical models relate K with electrical properties (including complex conductivity information) for natural aquifer materials, we generated laboratory samples for hydraulic and SIP electrical measurements on a range of stratigraphic units from the well-documented unconsolidated coarse fluvial aquifer at the Boise Hydrogeophysical Research Site (BHRS) [*Barrash and Clemo*, 2002; *Barrash and Reboulet*, 2004]. For context, we briefly describe the BHRS and supporting data sets and archived core used for selection and construction of laboratory samples in this study, and for evaluation of the quality of the laboratory samples.

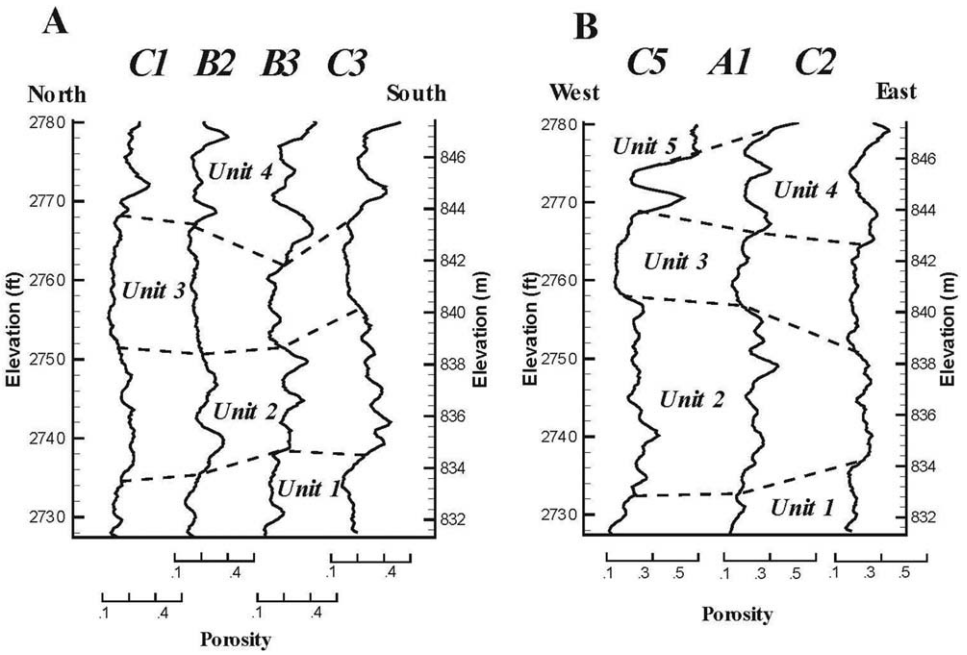

Figure 3. Stratigraphy in the shallow aquifer, as defined from porosity logs and core analysis [*Barrash and Clemo*, 2002; *Barrash and Reboulet*, 2004], includes four cobble-dominated units (Units 1–4, with unit numbers following depositional sequence from older to younger), overlain by a sand channel (Unit 5) that thickens toward the Boise River and pinches out in the center of the well field: (a) north-south transect; (b) east-west transect [after *Barrash and Clemo*, 2002].

The BHRS is located on a gravel bar adjacent to the Boise River 15 km southeast of downtown Boise, Idaho. The unconfined aquifer at the BHRS consists of ~20 m of mixed cobble, gravel, and sand fluvial deposits overlying a clay aquitard. Eighteen wells were cored through the unconsolidated, cobble, and sand fluvial deposits and completed into the underlying clay with screen through the aquifer. Of the 18 wells, 13 wells are arranged in two concentric rings (the B and C wells) around a central well (A1) in the 20 m diameter central area of the BHRS, and an outer ring of five "boundary" wells (X wells) are at greater distance from the central area [*Barrash and Clemo*, 2002].

Coring was conducted by hammering a split spoon (6.03 cm ID barrel) into the sediments and greater than 80% of well length was recovered. While some large grains were broken or truncated and original positions were not retained for grains relative to each other, it is unlikely that there was significant vertical sample mixing as generally occurs with auger or rotary drilling. This lack of vertical mixing is also supported by the recognition of five core sample types or lithotypes that are the sedimentological building blocks of the coarse fluvial aquifer [*Reboulet and Barrash*, 2003; *Barrash and Reboulet*, 2004]. The systematic occurrence of these lithotypes between and within the larger stratigraphic units (described below), including vertical transition probability for stratigraphic units, is further evidence that the core samples largely retain original sedimentary proportions and are not random mixtures.

Stratigraphy in the shallow aquifer, initially recognized from porosity logs and core analysis [*Barrash and Clemo*, 2002; *Barrash and Reboulet*, 2004], includes four cobble-dominated units (Units 1–4, with unit numbers following depositional sequence from older to younger), which are overlain by a sand channel (Unit 5) that thickens toward the Boise River and pinches out in the center of the well field (Figure 3). Units 1 and 3 have relatively low average porosity and low porosity variance. Units 2 and 4 have higher average and more variable porosity, whereas the Unit 5 sand deposit has the highest porosity and highest variance in porosity. Cross-well and borehole surveys using ground penetrating radar (GPR), seismic, and electrical resistivity methods have recognized a similar distribution of units suggesting that geophysical responses are largely consistent with observed porosity [e.g., *Clement et al*., 2006; *Moret et al*., 2006; *Mwenifumbo et al*., 2009].

For this study, 12 core samples were analyzed from four of the five stratigraphic units and from 10 of the 13 central area wells (Table 1) to represent lithologic and packing (porosity) variation observed in the aquifer

Table 1. Summary of Structural Characteristics of the 12 Reconstituted Unconsolidated Samples Examined in This Study[a]

Sample	Well	Unit	Lithotype[b]	K (m/s)	ø (%)	$ø_m$ (%)	F	σ'_{surf} (S/m)	σ'' (S/m)	Full GSD			Matrix GSD		
										d_{10} (mm)	d_{60} (mm)	E_h (m^{-1})	$d_{10[m]}$ (mm)	$d_{60[m]}$ (mm)	$E_{h[m]}$ (m^{-1})
1	B1	2	L	3.23E-04	17.0	33.0	12.5	7.46E-04	8.43E-06	0.44	26.22	6446	0.20	1.56	778
2	B2	2	L	6.88E-04	15.4	34.3	9.4	2.01E-04	3.47E-06	0.48	32.68	6359	0.23	1.91	870
3	B3	4	L	4.39E-04	12.2	27.5	11.5	3.65E-04	9E-06	0.46	36.93	4926	0.21	1.81	803
4	B4	1	M	6.28E-04	19.7	35.7	10.3	6.55E-04	9.77E-06	0.44	23.97	4812	0.23	1.87	898
5	B6	1	M	2.79E-04	14.4	25.8	13.4	6.31E-04	1.74E-05	0.41	23.27	3827	0.24	1.18	682
6	C1	2	M	2.20E-04	17.8	30.1	11.9	6.93E-04	1.27E-05	0.35	20.87	3052	0.21	1.01	581
7	C2	1	L	2.47E-04	16.4	36.4	13.3	5.77E-04	8.36E-06	0.49	35.11	6117	0.23	1.91	870
8	C3	2	L (M)	3.22E-04	17.0	32.0	13.0	3.89E-04	9.56E-06	0.36	24.57	4654	0.19	1.59	750
9	C3	4	M (L)	3.63E-04	21.9	39.3	7.7	2.47E-04	1.06E-05	0.32	28.63	3893	0.18	0.89	485
10	C4	5	S,F	6.57E-04	35.1	35.1	4.6	4.02E-04	1.71E-05	0.25	0.73	394	0.24	0.73	394
11	C5	2	M (L)	5.77E-04	16.9	32.9	10.3	5.13E-04	1E-05	0.38	24.10	4875	0.19	1.97	821
12	C5	5	F	6.06E-04	37.6	38.2	3.5	2.49E-03	1.27E-05	0.27	0.82	464	0.26	0.81	440
Average				4.46E-04	20.1	33.4	10.1	6.59E-04	1.08E-05	0.39	23.16	4152	0.22	1.44	698
Standard deviation (σ_d)				1.75E-04	8.0	4.1	3.3	6.01E-04	3.84E-06	0.08	11.57	2021	0.03	0.48	179

[a] K = hydraulic conductivity; ø = porosity; $ø_m$ = matrix porosity; F = formation factor; σ'_{surf} = real part of surface conductivity estimated from equation (4); σ'' = imaginary conductivity at 1 Hz; d_{10} and d_{60} are grain size diameters for which 10% and 60% of the sample are finer by weight, respectively; E_h = GSD integral calculated from equation (9); subscript [m] indicates values calculated for the matrix only.

[b] After *Barrash and Reboulet* [2004].

at the BHRS. An additional criterion for selection of specific samples was the presence of contiguous core with similar porosity (based on averaging of neutron log measurements over the well interval for a given sample) and similar cobble-to-matrix proportion characteristics of sufficient volume to completely or almost completely fill the sample volume. For sample preparation, however, truncated or broken cobbles from the original core samples were not used in order to avoid unnatural shapes and rough surface geometry that could affect hydrologic flow and electrical behavior. Instead, a comparable volume of similar size whole cobbles was substituted on a sample-by-sample basis. In a somewhat similar manner, supporting information was added to complete several samples; supporting information was prepared to have appropriate GSD proportions for a given sample. For several samples (Table 1), lithologic types were mixed to achieve a laboratory sample with sufficient matrix that maintained matrix and porosity characteristics even if source core samples might include lithotypes with broader cobble size distribution.

To provide independent perspective on the K measurements on laboratory samples for this study (see below), results from high-resolution multilevel slug tests [*Cardiff et al*., 2011; *Barrash and Cardiff*, 2013] and hydraulic tomography [*Cardiff et al*., 2013] are available for comparison. These measurements, along with KC estimates based on grain size and porosity characteristics, suggest that there are greater than 2 orders of magnitude of variation in K across the identified units (see below). However, as described below, the samples acquired for this study do not span this entire range.

4. Methods

We designed and constructed a device for measuring K and complex conductivity on reconstituted samples (Figure 4). Unconsolidated soils were packed into a flexible sock (nominal 0.102 m internal diameter and axis length 0.12 m) that could incorporate the cobble framework by accepting cobbles with a long axis up to 0.12 m (Figure 4). The laboratory sample dimensions are small relative to actual cobble dimensions in many cases, and only one or a few relatively "large" cobbles could be included in any given laboratory sample. Therefore, the samples were carefully packed to honor as closely as possible the core sample's cobble-to-matrix proportion with a similar overall porosity as obtained from borehole logging and GSD analysis of core material from the site. In placing cobbles in the sample, long axes of grains were aligned generally with the long axis of the sample to imitate orientations in relation to flow in the aquifer.

Following construction within the sock, each sample was placed in a 0.122 m PVC mould and a casting resin was used to form a hydraulic seal between the sock and the edge of the mould. The mould was then interfaced with end caps designed to permit measurements of both K and σ^* at the same scale (Figure 4). The end caps contained manometers for determining the head drop across the sample when interfaced with a

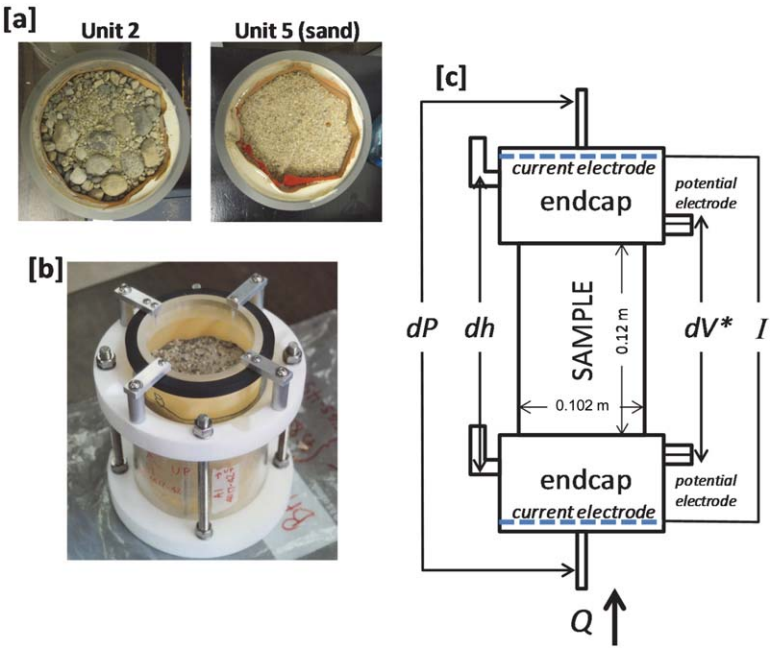

Figure 4. (a) Photos showing examples of reconstituted samples prepared in mould; (b) flexible sample holder used to prepare the samples; (c) schematic of the apparatus utilized for the joint measurement of hydraulic conductivity and complex conductivity (*dP* = pressure gradient driving flow, *dh* = head drop across sample for Darcy calculation, *dV** = complex voltage recorded in response to current flow (*I*)).

constant flow device for estimating *K* from Darcy's Law. The end caps each contained two electrodes for performing the four electrode σ^* measurement. Silver (Ag) spiral electrodes (0.076 m diameter) were housed at the back of the end cap (furthest from the sample) and used to encourage 1-D current flow along the sample. Point Ag-AgCl electrodes were used to record the sample complex impedance.

Samples were subsequently saturated with a NaCl solution adjusted to have an electrical conductivity (σ_w) of ~200 μS/cm, being representative of the groundwater at the BHRS [e.g., *Hausrath et al*., 2002]. Hydraulic conductivity was measured using a constant head device appropriate for coarse granular materials. Measurements of the head drop across the sample were recorded for at least five different flow rates in order to assign uncertainty to the *K* estimate. Complex conductivity measurements were next acquired between 0.001 and 1000 Hz using a dynamic signal analyzer described elsewhere [e.g., *Slater and Lesmes*, 2002]. A swept sine method was used to generate a sine function at 60 frequencies (equally spaced in log frequency), and the impedance magnitude and phase shift were recorded as a function of frequency, from which $\sigma^*(\omega)$ was computed using the geometry of the sample apparatus.

Formation factor (*F*) was next determined from measurements of σ' as a function of σ_w (equation (4)). Each sample was flushed with a minimum of five NaCl salinities (equally spaced in log σ_w) between approximately 30 and 3000 μS/cm. Salinities were successively increased starting with the lowest salinity solution, and a minimum of five pore volumes were introduced for each salinity increment to ensure fullest possible replacement of the pore fluids before each new measurement. Figure 5 shows examples of the relationship between σ' and σ_w and the estimation of *F* and the real part of the surface conductivity (σ'_s) based on equation (4). Following completion of all *K*, σ^*, and *F* measurements, samples were extracted from the mould/sock device and total porosity ($\varnothing$) was estimated using a weight-loss-by-drying method. GSDs for the sample material were then determined via sieve analysis.

The predictive capability of the above-described *K* prediction models (equations (1), (3), (8), (13), and (16)) and the equations presented in *Revil and Florsch* [2010] (equations (14) and (15)) linking imaginary conductivity to the GSD were investigated under conditions when the cobble framework was included and when it was discounted. Cross plots of predicted versus measured parameters are presented, and the deviation $\bar{\sigma}_d$ of the model predictions from the measurements in log space computed as

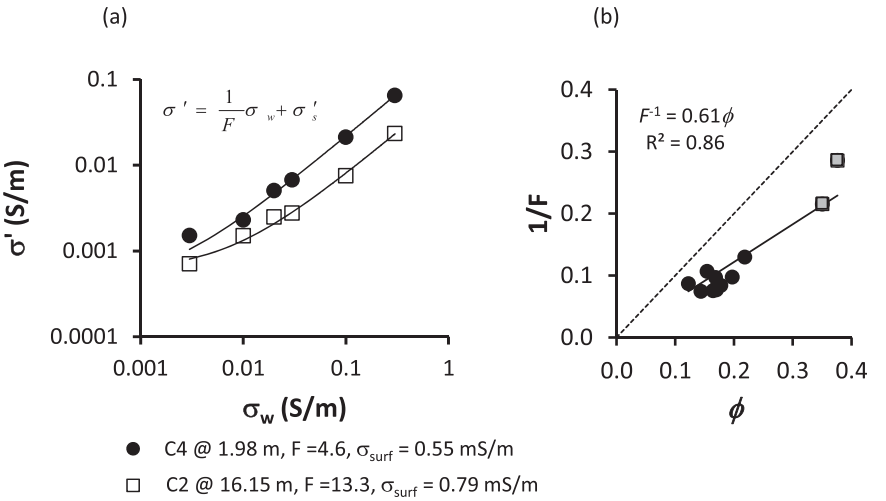

Figure 5. (a) Example plots of σ' versus σ_w for determining true formation factor of the samples. Filled circles represent a matrix-only sample whereas white circles represent a cobble framework sample. (b) Relationship between formation factor (F) and total porosity ($\varnothing$) for the 12 reconstituted samples examined in this study. Best line equation and coefficient of determination (R^2) are shown, along with the deviation from the 1:1 relation expected from $1/F = \varnothing_{eff}$ and assuming $\varnothing_{eff} \cong \varnothing$ for these coarse materials. In Figure 5b, gray squares represent matrix only (Unit 5) samples, whereas black circles are samples containing a cobble framework.

$$\bar{\sigma}_d = \frac{1}{n} \cdot \sum_{j=1}^{n} \left| \log_{10}(X_j) - \log_{10}(X_j^*) \right|, \tag{17}$$

where X represents a measured property (either K or σ''), X^* is the model estimate for that property, and n is the number of data points (12 in each case). We also calculated the Akaike Information Criterion (AIC), a popular approach in chi-squared data fitting to select among different models (with differing numbers of parameters (k)) where the likelihood functions assume that the underlying errors are normally distributed (with zero mean) and independent. The AIC was calculated from the residual sum of squares (RSS) according to

$$AIC = n \ln \frac{RSS}{n} + 2k + C, \tag{18}$$

where C is a constant that is ignored for model comparisons as performed here. More negative AIC values indicate a relatively higher-quality model compared to the others tested.

5. Results

5.1. Physical Properties

Table 1 summarizes the major physical properties of the twelve samples, including lithotype defined by *Barrash and Reboulet* [2004], $\varnothing$, F, K, σ'_{surf} calculated from equation (4), σ'' at 1 Hz, characteristic grain diameters (d_{60} and d_{10}), and grain size integral (E_h) calculated from equation (9). In addition to total porosity, matrix-only porosity ($\varnothing_m$) is also shown. Characteristic grain diameters for the matrix-only ($d_{10[m]}$, $d_{60[m]}$) and matrix-only grain size integral ($E_{h[m]}$) are also included. The K estimates from Darcy tests only vary by a factor of $\sim$3 and do not capture the $>$2 orders of magnitude variation observed in field-scale slug tests [*Cardiff et al.*, 2011; *Barrash and Cardiff*, 2013]. The inclusion of the cobble framework results in a large porosity decrease relative to the sand samples (Unit 5). Porosity varies from a minimum of 12.2% in a cobble-dominated sample from Unit 4, to a maximum of 37.6% for the two samples from the sand (Unit 5). The cobble framework also increases F due to its effect on both reducing the pore space volume and increasing the tortuosity of the electrical current flow paths. The relationship between F and $\varnothing$ follows Archie's Law [*Archie*, 1942], $F = \varnothing^{-m}$, with a cementation exponent (m) equal to 1.34 (linear coefficient of determination (R^2) of the least squares regression is 0.82) which is similar to a previous field estimate at the BHRS

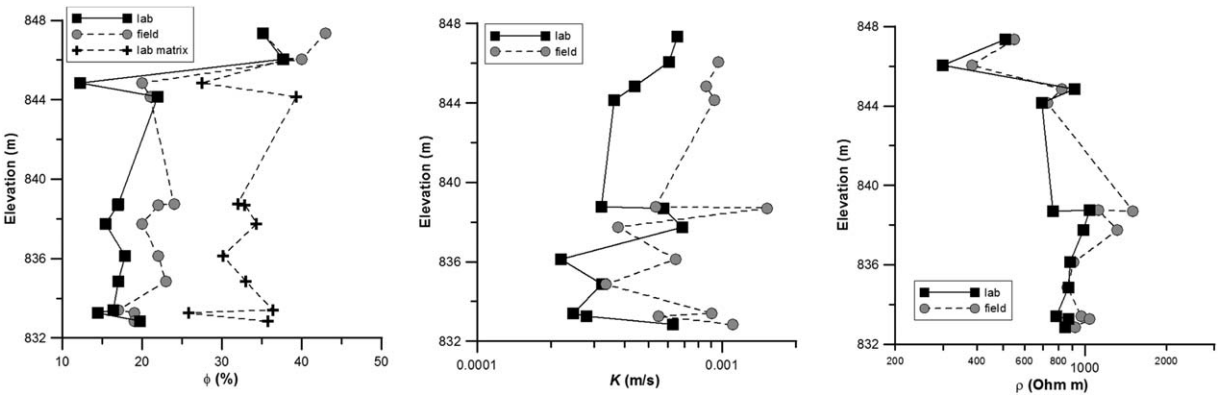

Figure 6. Comparison of laboratory and field-scale estimates of physical properties: (a) porosity ($\varnothing$) (laboratory-derived total and matrix porosity shown); (b) hydraulic conductivity (K); (c) resistivity (ρ) corrected to 18°C.

[*Oldenborger et al*., 2007], and is within the range of reported values at a site in a similar aquifer in downtown Boise about 15 km from the BHRS [*Barrash et al*., 1997]. As previously noted, F senses the electrically connected porosity ($\varnothing_{eff}$) [*Revil and Cathles*, 1999]. Figure 5b shows the relationship between $\varnothing$ and F fitted to equation (7). Formation factors for laboratory samples (Table 1) are similar to those reported by *Oldenborger et al*. [2007] from field data. Assuming that $\varnothing_{eff} \cong \varnothing$ in these coarse grained, unconsolidated sediments, the deviation of the data points from the 1:1 line can be accounted for by an electrical tortuosity (τ) = 1/0.61 = 1.64.

The standard deviation (σ_d) of the characteristic grain diameter d_{10} including the cobble framework is only 0.08 mm because the d_{10} grain size lies within the sand matrix fraction of the GSD, whereas σ_d of d_{60} (cobble framework included) is 11.6 mm due to the large size range of the framework fraction. The σ_d of the grain size integral (E_h) for the sample with cobble framework included is 2021 m^{-1} due to the strong influence of the coarse cobble fraction. The standard deviations for the equivalent parameters for the matrix only are much smaller, being 0.02, 0.48, and 179 m^{-1} for $d_{10[m]}$, $d_{60[m]}$, and $E_{h[m]}$, respectively.

5.2. Comparison With Field Data

Figure 6 compares laboratory-derived physical properties with estimates available from field-scale measurements at the BHRS. These field-scale measurements are total porosity from neutron logs [*Barrash and Clemo*, 2002], hydraulic conductivity from slug tests [*Cardiff et al*., 2011; *Barrash and Cardiff*, 2013], and resistivity from capacitive resistivity logging [*Mwenifumbo et al*., 2009]. Profiles of laboratory measurements are plotted against the field-derived estimates from the position closest to where the sample was taken in Figure 6. The shapes of the field and laboratory-determined porosity profiles are very similar, although laboratory-derived porosity is generally lower than the field estimate. This likely reflects settling or slightly greater compaction of the sediments in the sample holder (during shipping and handling) relative to the in situ conditions. The profile of estimated matrix porosity is also shown and indicates that the porosity through which fluid flow occurs varies from 30 to 45%.

Hydraulic conductivity profiles from the field and laboratory are also generally consistent with each other except for the data point at an elevation of 836 m. The generally lower K determined in the laboratory again likely indicates the effect of compaction of these samples. Given the challenges of reconstituting the physical properties of unconsolidated samples with a broad GSD, we consider the general correspondence between laboratory and field estimates of K very encouraging, particularly given the different support volumes of these two measurements. Although significant anisotropy is not expected, the slug tests will be most sensitive to the horizontal component of K and lab samples were reconstituted with long axes of cobbles parallel to sample-cell axis to measure horizontal K. Our observations are consistent with the fact that K is often observed to increase with support volume between laboratory and field scales [e.g., *Zlotnik et al*., 2000].

The profiles of laboratory and field resistivity values are very similar after correction for differences in temperature between in situ groundwater (12.8°C ± 0.5°C) and pore fluid in the laboratory (22°C ± 0.5°C).

Figure 6c compares resistivity of the laboratory samples with capacitive resistivity at the sampled location after both measurements are corrected to a reference temperature of 18°C using the relationship, $\rho_w(18)=\rho_w(T)[1+\alpha(T-18)]$, where α is an empirical coefficient typically equal to 0.025°C^{-1} [*Keller and Frischknecht*, 1966]. Excluding one obvious outlier at 838 m elevation, linear regression of the field-scale resistivity from the capacitive log (ρ_{field}) against the laboratory sample resistivity (ρ_{lab}) results in the relation $\rho_{field} = 1.1\ \rho_{lab}$, with a coefficient of determination (R^2) equal to 0.81. The overall slightly higher resistivity recorded in the field may reflect the sensitivity of the capacitive resistivity log to the larger cobble fraction than could be included in the 0.102 m diameter sample holders [*Mwenifumbo et al.*, 2009]. The outlier at 838 m may similarly be attributed to the laboratory sample not adequately capturing the cobble framework at this location.

Given the limitations of reconstituting representative samples of unconsolidated sediments in the presence of a broad GSD that includes a cobble framework, the field and laboratory estimates of available physical properties are generally consistent. This finding provides a basis for comparison of the electrical and hydraulic properties of the laboratory samples that has significance for understanding field-scale electrical-hydraulic relations.

5.3. Comparison With Kozeny-Carman (KC) Estimates

Figures 7 and 8 compare the laboratory-measured K with various KC estimates based on the sample physical characteristics reported in Table 1. Figure 7 shows cross plots of estimated versus measured K for KC estimates, (1) considering the full GSD as per equation (1) (K_{KC}) and (2) discounting for the cobble framework as per equation (3) ($K_{KC[mod]}$). The K_{KC} estimates for the sand (Unit 5) are shown as gray symbols and are in close agreement with the laboratory-measured values. However, for all units that contain a cobble framework, K_{KC} underpredicts the laboratory measurements by on average a little under an order of magnitude ($\bar{\sigma}_d$ =0.83 considering the 10 cobble samples alone, $\bar{\sigma}_d$=0.74 for all 12 samples). Discounting for the cobble framework ($K_{KC[mod]}$) improves the K estimates, although the improvement is marginal ($\bar{\sigma}_d$=0.65 considering the 10 cobble samples alone, $\bar{\sigma}_d$=0.58 for all 12 samples). It appears that the larger d_{10} but lower ø associated with the full GSD (K_{KC}) is largely offset by the higher ø but smaller $d_{10[m]}$ for the matrix when the cobble volume percent discount is applied to determine $K_{KC[mod]}$.

Figure 8 shows vertical profiles of K measured versus K_{KC}, $K_{KC[mod]}$, and the KC estimate for the hydraulic conductivity of the matrix (K_m) as per equation (2). The K_m values provide a closer estimate of the laboratory-measured values than K_{KC} or $K_{KC[mod]}$ ($\bar{\sigma}_d$ =0.42) suggesting a relatively greater influence of the matrix than is incorporated into the modified KC equation (3). However, K_m physically should not represent the hydraulic conductivity of the core sample as the cobbles are ignored. Instead, K_m can be considered an upper possible limit to the K estimate from KC using d_{10} as the effective grain size. Possible explanations for the significant offset between $K_{KC[mod]}$ and laboratory-measured K include: (1) the discounting for large grains is not strictly linear [e.g., *Koltermann and Gorelick*, 1995; *Barrash and Cardiff*, 2013], as assumed in our model here and (2) d_{10} is smaller than the "true" effective grain size for KC in these sediments. The latter explanation is partly supported by the fact that both KC approaches are biased low relative to the Darcy laboratory profile.

Another explanation for the weak correspondence between $K_{KC[mod]}$ and measured K is that equation (3) does not account for the extra tortuosity due to the "twists and turns" that the continuous matrix "capillaries" must take to get around the framework cobbles. This tortuosity is in addition to the tortuosity associated with flow paths around grains that is included in the KC equation [see *Carman*, 1937; *Charbeneau*, 2000]. The additional tortuosity accounts for the fact that the interconnected matrix bodies (supporting flow) occur in the interstices between cobble framework grains and these matrix bodies or "matrix capillaries" also follow tortuous paths around the cobbles. Table 1 indicates that the electrical formation factor and the total porosity are strongly controlled by the presence of the cobbles. The electrical tortuosity (τ) is commonly computed as $\tau = F/ø$. Figure 8 therefore also shows the profile of $K_{KC[mod]} \times \tau$. This results in the best estimate of K ($\bar{\sigma}_d$ =0.42) relative to estimates obtained using $K_{KC,}$ $K_{KC[mod]}$, or K_m. The benefits of including electrical measurements sensitive to the effective porosity and accounting for the tortuosity of flow paths has already been discussed. The findings supports the concept that τ primarily represents the tortuosity of the matrix "capillaries" around the cobbles.

$$K_{KC} = \frac{\rho_w g}{\mu} \frac{\emptyset^3 d_{10}^2}{180(1-\emptyset^2)}$$

(a)

$$K_{KC[mod]} = K_m(\emptyset + V_m)$$

$$K_m = \frac{\rho_w g}{\mu} \frac{\emptyset_m^3 d_{10[m]}^2}{180(1-\emptyset_m)^2}$$

(b)

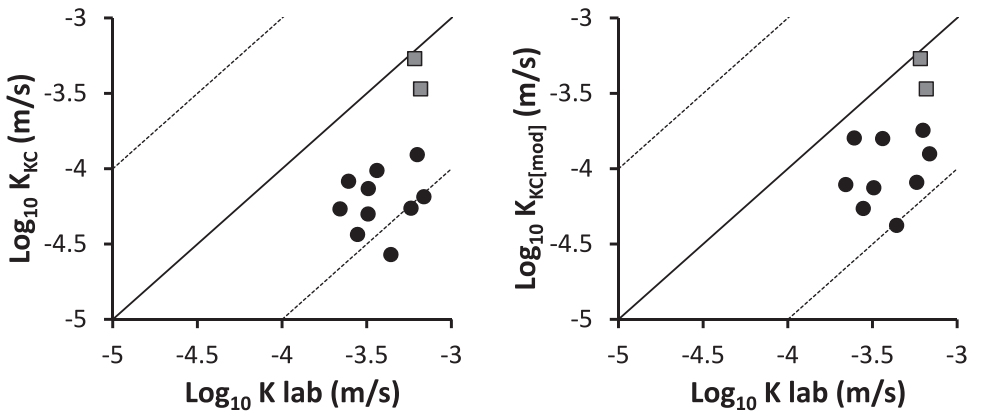

Figure 7. Predicted hydraulic conductivity from the Kozeny-Carman model versus hydraulic conductivity measured using Darcy lab tests: (a) without discounting for the cobble framework ($\bar{\sigma}_d$ =0.74, AIC = −2.63); (b) discounting for the cobble framework ($\bar{\sigma}_d$=0.58, AIC = −5.43). The 1:1 line (solid line) and the lines for $\bar{\sigma}_d$ =±1 (dashed lines) are shown to guide the eyes. Gray squares represent matrix only samples, whereas black circles are samples containing a cobble framework.

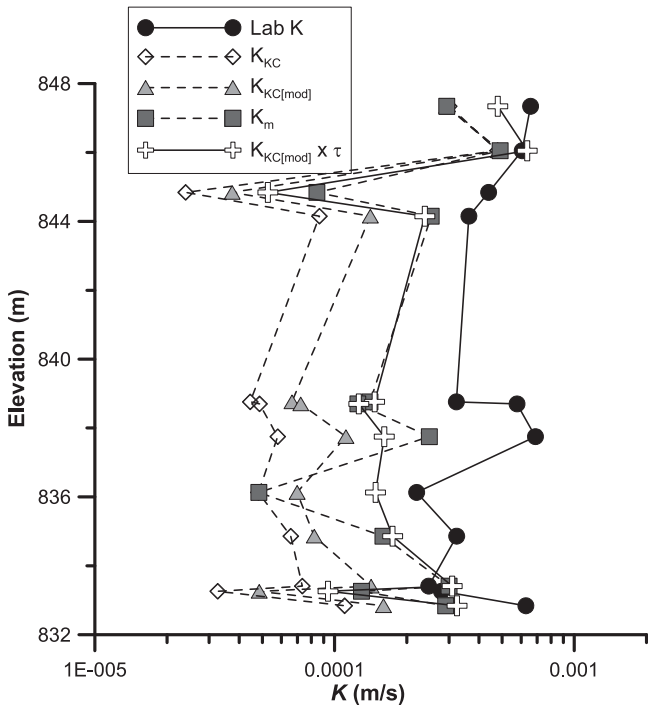

Figure 8. Comparison of Kozeny-Carman estimates of *K* versus laboratory-derived *K* from Darcy tests. Plotted are KC estimates based on: (1) the full sample GSD (K_{KC}) as per equation (1) ($\bar{\sigma}_d$=0.74, AIC = −2.62); (2) discounting for the cobble framework ($K_{KC[mod]}$) as per equation (3) ($\bar{\sigma}_d$=0.58, AIC = −5.43); (3) matrix-only *K* (K_m) based on equation (2) ($\bar{\sigma}_d$=0.42, AIC = −9.79); (4) $K_{KC[mod]}$ x τ, where $\tau = F/\emptyset$ ($\bar{\sigma}_d$=0.35, AIC = −14.00).

It is clear that the overall relative *K* trends in the Darcy laboratory profile are retained to similar degrees in the K_{KC} and $K_{KC[mod]}$ profiles. Therefore, KC estimates provide reasonable estimates of relative *K*, but need to be scaled by either or both (a) the "true" effective grain size for the sediment type, or (b) the "true" "hydraulic discount rate" for the cobble portion of the GSD because the cobble framework grains do not effectively surround flow "capillaries" as in the Kozeny-Carman conceptual model, but rather effectively block available flow volume or cross section in the fractional packing sense [e.g., *Koltermann and Gorelick*, 1995].

5.4. Complex Conductivity Spectra

Only subtle variations were observed in the complex conductivity (σ^*) spectra between samples representative of the different units at the BHRS. Figure

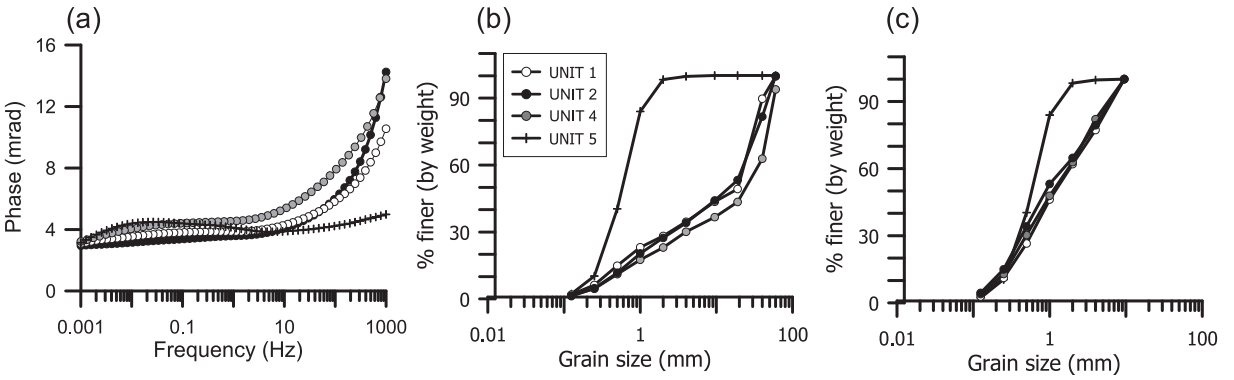

Figure 9. Comparison of units based on representative samples: (a) complex conductivity spectra; (b) full GSD; (c) GSD of matrix only.

9a shows measured phase spectra for one sample from each unit covered by the samples listed in Table 1. The corresponding full GSDs and GSDs with the cobble framework discounted are shown in Figures 9b and 9c, respectively. The spectra for all units are characterized by phase between 3 and 5 mrad below 10 Hz, with higher and more variable values between 10 and 1000 Hz. The polarization of the Stern layer (i.e., as described by equations (5) and (6)) is assumed to dominate the complex conductivity response below 10 Hz, whereas an additional contribution from the Maxwell-Wagner interfacial polarization is assumed to partly explain the increase in phase beyond 10 Hz. It is possible that polarization errors due to the capacitive effects of the circuit represented by the potential electrodes and associated connections also contributes to this phase increase, although calibrations on water samples matching the resistance of the sediments indicate that this error is no more than 3 mrad at 1000 Hz.

Below 10 Hz, small differences in the shape of the phase spectra between units can be observed. The sand unit (Unit 5) shows a pronounced phase peak between 0.01 and 1 Hz. The samples containing the cobble framework exhibit weaker ϕ peaks below 10 Hz, with the sample from Unit 2 showing no evidence of a peak, but instead showing a continuous increase in phase from 0.001 Hz to 10 Hz. The more pronounced peak for the well-sorted sand sample (Figure 9b) is consistent with the GSD model that assumes the polarization can be represented by the integral of a distribution of Debye relaxations across the distribution of grains making up the matrix of the porous material. In this model, well-sorted samples should exhibit a distinct polarization peak at a frequency related to a dominant relaxation time centered on the mean grain size of the material. In contrast, material characterized by a broad distribution of grain sizes will be characterized by a broad distribution of relaxation times and therefore be devoid of a peak in the frequency spectrum. The weaker polarization peaks in the samples containing the cobble framework are consistent with this expectation.

However, we should expect a negligible contribution of the cobbles to the polarization observed across our measured frequency range. The time constant of the relaxation associated with a single grain is proportional to the square of the grain diameter (equation (6)). Assuming a representative diffusion coefficient (D_i) of 1.3×10^{-9} m^2 s^{-1} [e.g., *Revil et al*., 2012], the time constant (τ_0) for a grain diameter of 10 mm (i.e., the lower cutoff for the cobble fraction, see above) is 5063 s ($1/\tau_0 = 2 \times 10^{-4}$ s) (equation (6)). Therefore, the polarization of the EDL around the cobbles in our samples would be observed at frequencies well below 0.001 Hz, being the lower end of the measured frequency range. A bimodal distribution of relaxation times would then be expected if it were possible to measure to low enough frequencies to capture the polarization response of the cobbles. Although a small contribution to the polarization at the lowest measurement frequencies could result from the breadth of the measured polarization response of the cobbles, we have insufficient information to resolve this in the data.

The GSDs shown in Figure 9 serve to illustrate the structural similarity of the units containing the cobble fraction. The full GSD for the sample from the sand unit is distinctly different from the full GSD for the units containing a cobble fraction (Figure 9b). However, Figure 9c illustrates that the sand samples are structurally similar to the matrix portion of samples containing the cobble fraction (i.e., when the GSD distribution

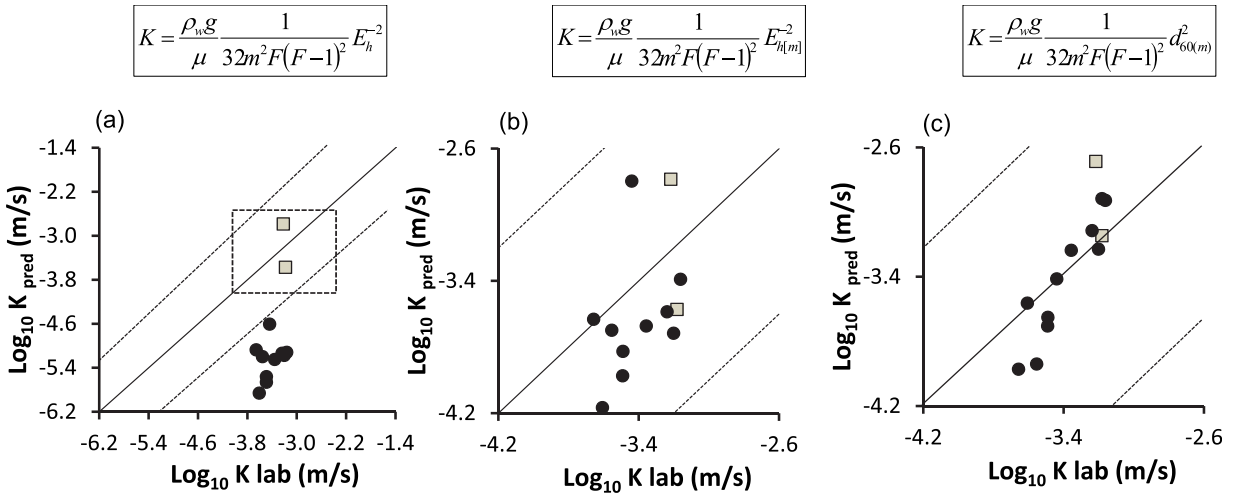

Figure 10. Predicted hydraulic conductivity from the *Revil and Florsch* [2010] model versus hydraulic conductivity measured using Darcy lab tests: (a) using the full GSD (E_h) ($\bar{\sigma}_d$ = 1.6, AIC = 18.96); (b) using the matrix-only GSD ($E_{h(m)}$) ($\bar{\sigma}_d$ = 0.55, AIC = −1.10); (c) using an effective grain size of the matrix only (in this case $d_{60(m)}$) in place of $E_{h(m)}$ ($\bar{\sigma}_d$ = 0.24, AIC = −19.77). Gray squares represent matrix only samples, whereas black circles are samples containing a cobble framework. The 1:1 line (solid line) and the lines for $\bar{\sigma}_d = \pm 1$ (dashed lines) are shown to guide the eyes. The dashed box shown in Figure 10a depicts the bounds of the *x* and *y* axis scales shown in Figures 10b and 10c.

excluding the cobble fraction is considered). All samples show negligible silt and clay which is common for these high-energy deposits [*Reboulet and Barrash*, 2003; *Barrash and Reboulet*, 2004; *Carling and Reader*, 1982; *Church et al.*, 1987; *Lord and Kehew*, 1987; *Paola and Seal*, 1995; *Heinz*, 2001] and may be significant for *K* behavior (see below). The subtle difference between the ϕ spectrum of the sand sample and the ϕ spectra for the samples containing the cobble fraction indicates that σ^* is insensitive to the cobble framework. The fact that the cobble framework polarizes outside of the frequencies recorded in SIP measurements is important for the prediction of the imaginary conductivity and the hydraulic conductivity from the Stern layer polarization model as illustrated later.

5.5. *K* Estimates From Formation Factor and Grain Size Distribution

Figure 10a compares *K* measured in the laboratory with *K* predicted (K_{pred}) from equation (8), based on E_h calculated for the full GSD and not discounting of the cobble framework. While laboratory-measured *K* only varies by a factor of 3, K_{pred} varies by approximately 3 orders of magnitude. While K_{pred} is within the right order of magnitude for the sand samples, K_{pred} for the samples containing the cobble framework is approximately 2 orders of magnitude lower than measured *K* ($\bar{\sigma}_d$ = 1.6). This observation is consistent with the concept that E_h does not represent the effective grain sizes controlling fluid flow when the full, multimodal, non-log normal, GSD incorporating the cobble framework is considered.

Figure 10b compares *K* measured in the laboratory with *K* estimated from equation (8) based on the matrix-only GSD $E_{h[m]}$ (i.e., with the cobble framework discounted). The predicted values for the two sandy samples of Unit 5 are unchanged as $E_{h[m]} = E_h$. However, the predicted *K* values for the samples containing the cobble framework are now well less than an order of magnitude from the measured values ($\bar{\sigma}_d$ = 0.55). Predicted *K* values for the 10 samples containing the cobble framework mostly fall below the measured values. Similar to the classical Kozeny-Carman formulation, this comparison of Figures 10a and 10b provides evidence of the need to discount for the cobble framework in the prediction of *K* when using the formation factor and GSD integral as per equation (8).

Figures 7b and 10b compare the results of a Kozeny-Carman model formulated in terms of porosity and grain size parameters with a model formulated based on the electrical formation factor and grain size parameters, the cobble framework being discounted in both cases. The improvement observed in Figure 10b is likely partly due to the use of the electrical formation factor (*F*) rather than the total porosity, as *F* senses the effective porosity ($\varnothing_{eff}$), being the product of the total interconnected porosity and the tortuosity (τ) of the current flow paths. The control of the cobble framework on *F* is obvious in Table 1. While the two sandy samples have formation factors of 3.5 and 4.5, formation factors for the samples containing the cobble framework vary from 6.2 to 12.6. Figure 10b suggests that the use of the formation factor, combined

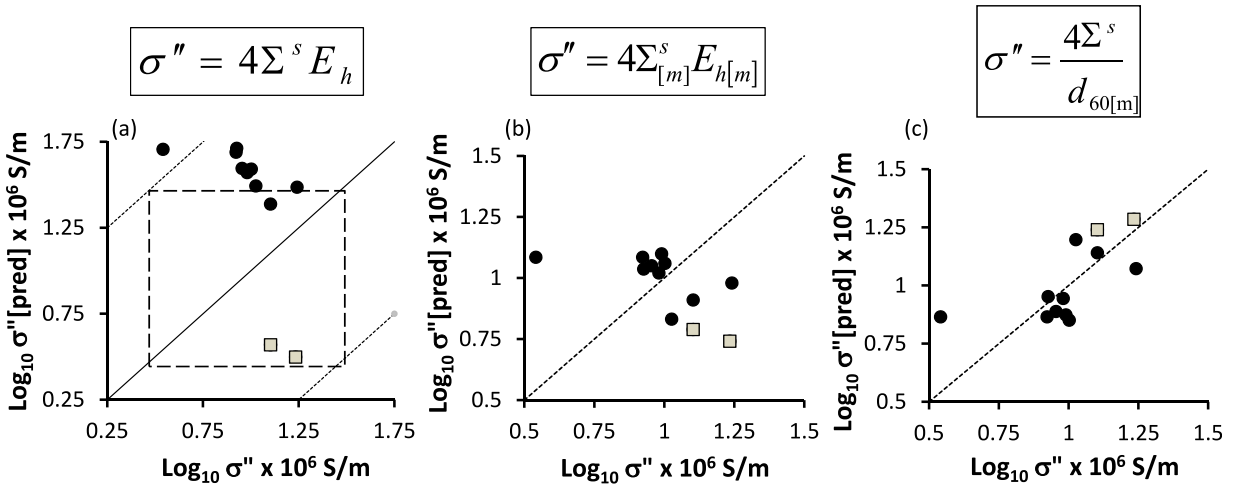

Figure 11. Predicted imaginary conductivity from the *Revil and Florsch* [2010] model versus imaginary conductivity at 1 Hz measured in the laboratory: (a) using the full GSD (E_h) ($\bar{\sigma}_d$ =0.62, AIC = −6.01); (b) using the matrix-only GSD ($E_{h[m]}$) ($\bar{\sigma}_d$ =0.21, AIC = −27.80); (c) using an effective grain size of the matrix only (in this case $d_{60(m)}$) in place of $E_{h[m]}$ ($\bar{\sigma}_d$ =0.11, AIC = −41.37). The 1:1 line is shown in both figures to guide the eyes. The dashed box shown Figure 11a depicts the bounds of the *x* and *y* axis scales shown in Figures 11b and 11c. Gray squares represent matrix only (Unit 5) samples, whereas black circles are samples containing a cobble framework.

with the discounting of the porosity of the cobble framework, as per equation (3), effectively compensates for the volume of the cobbles that do not contribute to flow. In these unconsolidated, uncompacted, coarse, loose materials with virtually no silt or clay, the effective porosity of the matrix will likely be close to the total porosity of the matrix (equation (7)). The clear improvement in *K* prediction when using an electrical formation factor in place of porosity most likely results from the sensitivity of *F* to the tortuosity of the electrical current and (by analogy) matrix "capillaries" around the cobbles.

Figure 10c shows a modification to equation (8) as given by the approximation shown in equation (12), whereby the grain size integral has been replaced by an effective grain diameter for the matrix ($d_{eff[m]}$), where in this case $d_{60[m]}$ is used as it provided a significantly improved fit to the measured *K* values compared to using measures of the finer part of the GSD, e.g., $d_{10[m]}$. This follows from physical intuition for such coarse materials, where fines (silt and clay) are absent (Figures 10b and 10c) [*Barrash and Reboulet*, 2004, and references therein] and *K* might be expected then to be influenced by a larger representative grain size such as d_{60}, which is a recognized index value for the larger fraction in a GSD as in the commonly used uniformity coefficient metric [e.g., *Kresic*, 1997]. Similar to the results obtained when exploring the fit to the Kozeny-Carman equation, this again suggests that d_{10} is smaller than the "true" effective grain size in these sediments. The use of $d_{60[m]}$ (Figure 10c) relative to $E_{h[m]}$ (Figure 10b) appears to reduce the scatter around the 1:1 line significantly ($\bar{\sigma}_d$ =0.24). Note that equation (13) is very similar in construction to equation (2), with the formation factor substituted for porosity.

5.6. Imaginary Conductivity Estimates From the Grain Size Distribution

Figure 11a compares σ'' measured in the laboratory at 1 Hz with σ'' estimated from equation (14) based on the full GSD and no discounting of the cobble framework. We assume $\Sigma^s = 4 \times 10^{-9}$ S at our fluid salinity range of 0.02 S/m, as found by *Boleve et al*. [2007] for glass beads over the salinity range 10^{-4} to 10^{-1} S/m. In this regard, sediments at the BHRS are silica-rich clasts derived from dominantly granitic source rock in the upper Boise River drainage basin [*Barrash et al*., 1997]. Considering the sand samples, the predicted σ'' is within half an order of magnitude of measured σ'' ($\bar{\sigma}_d$ =0.78). The predicted σ'' underestimates measured σ'' for these sand samples. Considering the samples containing the cobble framework, σ'' predicted is greater than half an order of magnitude from the measured σ'', with the predicted values overestimating the measurements.

Figure 11b compares σ'' measured in the laboratory at 1 Hz with σ'' estimated from equation (14) based on the matrix-only GSD (i.e., with the cobble framework discounted). Consistent with what is observed for *K*, the prediction of σ'' is improved by discounting for the cobble framework; with one exception, the predicted values fall close to the measured values ($\bar{\sigma}_d$ =0.21). Just as in the case for *K*, it appears necessary to

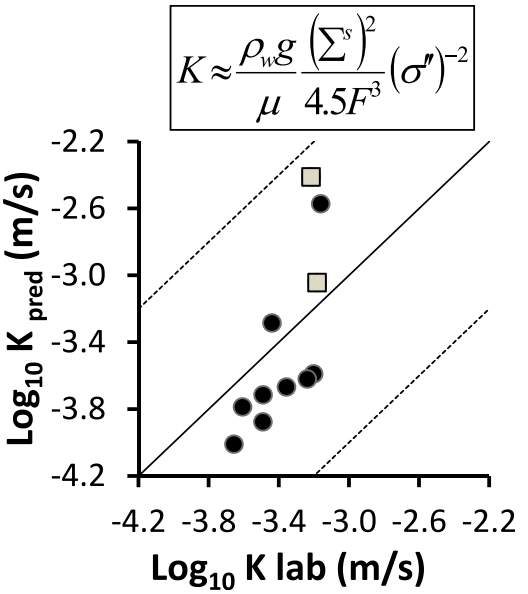

Figure 12. Predicted hydraulic conductivity from the *Revil and Florsch* [2010] model versus hydraulic conductivity measured using Darcy lab tests when imaginary conductivity is directly used for *K* estimation. The specific surface conductance of the Stern Layer (Σ^s) is assumed to equal 4E–09S ($\bar{\sigma}_d = 0.4$, AIC = −12.47). The 1:1 line (solid line) and the lines for $\bar{\sigma}_d = \pm 1$ (dashed lines) are shown to guide the eyes. Gray squares represent matrix only samples, whereas black circles are samples containing a cobble framework.

discount the cobble framework from the estimation of σ'' based on grain size models. This is consistent with the concept that we do not see the polarization of the cobbles across the limited frequency range of the measurements, as the cobbles polarize at much lower frequencies.

Figure 11c shows the fit for a modification to equation (14) as given by the approximation shown in equation (15), whereby the grain size integral has been replaced by an effective grain diameter for the matrix ($d_{eff[m]}$). In this case, $d_{60[m]}$ is used to be consistent with what was used in the *K* estimation described above. Furthermore, consistent with what was found for the *K* estimation, $d_{60[m]}$ provided a significantly improved fit to measured σ'' compared to using measures of the finer part of the GSD, e.g., $d_{10[m]}$. With one exception, the sand and cobble samples fall close to the 1:1 line ($\bar{\sigma}_d = 0.11$).

5.7. *K* Estimates From Imaginary Conductivity and Formation Factor

The relationship between σ'' and GSD affords the opportunity to estimate *K* from only electrical measurements. The predictive capability of equation (16), based on this substitution of σ'' as a proxy for GSD, is shown in Figure 12. The specific surface conductivity (Σ_s) was again set to 4×10^{-9} S. The predicted *K* falls within an order of magnitude of measured *K* for all samples, with 10 out of 12 samples having a predicted *K* within half an order of magnitude of measured *K* ($\bar{\sigma}_d = 0.4$). Based on $\bar{\sigma}_d$ alone, the prediction of *K* using this equation appears to be better than that obtained using both the cobble-discounted Kozeny-Carman equation (equation (3)) and the cobble-discounted equation using formation factor and grain size integral (*Eh*[*m*]) (equation (8)). However, the prediction using equation (16) is not as good as that obtained using formation factor and the effective grain diameter (in this case, $d_{60[m]}$). Table 2 summarizes the predictive performance of the *K* prediction models explored here.

6. Discussion

We have reported electrical and hydraulic measurements made on carefully reconstituted samples that incorporate a cobble framework. The broader significance of the findings of any laboratory study of soil samples is partly dependent on whether the recovered and reconstituted samples are representative of subsurface in situ conditions. The comparison of the laboratory-measured and field-measured physical properties suggests that the meticulously repacked samples were overall representative of physical properties occurring in the primary units at the BHRS.

Our measurements on these reconstituted samples indicate that *K* estimation from a traditional KC formulation is improved when effective grain size parameters are discounted for the cobble framework of these coarse unconsolidated sediments. However, this improvement alone is marginal. The matrix hydraulic conductivity (K_m) (equation (2)) was found to be a closer estimate of the measured *K*, suggesting a stronger influence of the matrix than is incorporated into the modified KC equation (3). This discrepancy may result from either or both (1) the discounting for large grains not being strictly linear as assumed, and (2) d_{10}

Table 2. Summary of the Results Obtained With the Different *K* (Kozeny-Carman (KC); Revil and Florsch (RF)) and σ'' (From Grain Size) Prediction Models as per the Average Deviation ($\bar{\sigma}_d$) of the Model Predictions From the Measurements in Log Space and the Akaike Information Criterion (AIC)[a]

Equation		Model Parameters	$\bar{\sigma}_d$	AIC
K Estimation				
KC	Equation (1)	ø, d_{50}	0.74	−2.62
$KC_{[mod]}$	Equation (3)	ø, $d_{50[m]}$	0.58	−5.43
Km	Equation (2)	ø, $d_{50[m]}$	0.42	−9.79
$KC_{[mod]} \times \tau$		ø, $d_{50[m]}$, F	0.35	−14.00
RF	Equation (8)	F, E_h	1.60	18.96
RF[mod]	Equation (8)	F, $E_{h[m]}$	0.55	−1.10
RF[mod]*	Equation (8)	F, $d_{eff[m]}$	0.24	−19.77
$RF_{[\sigma'']}$	Equation (16)	F, σ''	0.40	−12.47
σ'' *Estimation*				
Full GSD	Equation (14)	E_h, Σ_s	0.62	−6.01
Matrix GSD	Equation (14)	$E_{h[m]}$, Σ_s	0.21	−27.80
Effective grain size	Equation (15)	$d_{eff[m]}$, Σ_s	0.11	−41.37

[a]More negative AIC values indicate a relatively higher-quality model compared to the others tested. [mod] indicates that cobble framework was discounted; the asterisk indicates that an effective grain diameter for the matrix ($d_{eff[m]}$) was substituted for $E_{h[m]}$.

being smaller than the "true" effective grain size for KC in these sediments. The latter is supported by the fact that predictions with the SLP model suggest that d_{60} is a good measure of the effective grain size required for *K* prediction. Another issue is that the model applied assumes a simple arithmetic averaging of the saturated hydraulic conductivity of the matrix and the (impermeable) cobbles. Alternative formulae of greater complexity exist [*Cousin et al*., 2003; *Ma et al*., 2010] but do not benefit from an analogous electrical constitutive equation.

Multiplication of KC_{mod} by $\tau = F/ø$, assumed to represent the tortuosity of the matrix "capillaries" around the cobble framework, resulted in the best estimate of *K* from the KC formulation. This tortuosity is usually assumed to represent the "twists and turns" of interconnected pores within a rock or soil matrix. In our case, the cobble framework exerts a strong control on *F* and ø, supporting the concept that τ primarily represents the tortuosity of the matrix around the cobbles. The inclusion of electrical parameters sensitive to the tortuosity of the interconnected pores has previously been shown to result in improved estimates of *K* over conventional KC formulations [e.g., *Revil and Cathles*, 1999]. Our findings are consistent with this concept.

The formation factor is highly sensitive to the presence of the cobble framework as it dramatically reduces the available flow cross-section (i.e., a type of effective porosity reduction) in addition to increasing tortuosity; the two sand samples representing the matrix have F = 3.5–4.5, whereas the presence of the cobbles increases *F* to 6.5–12.5 (Table 1). This indicates that it is inappropriate to simply ignore the cobble framework, as might be inferred from the close correspondence between K_m and measured *K*. This would imply that the tortuosity calculated from the relationship $\tau = F/ø$ is representative of the capillary tortuosity of the matrix around the cobbles in these sediments, rather than the tortuosity of streamlines of pores through matrix.

The *K* predictions achieved with the *Revil and Florsch* [2010] model that directly includes *F* as a measure of the effective porosity ($F \approx 1/ø_{eff}$) are strongly dependent on discounting of the cobble framework. Applying equation (8) based on the grain size integral (E_h) and *F* without discounting for the cobbles results in the worst predictions of any model tested (Table 2). The use of $E_{h[m]}$ results in better *K* estimates relative to estimates obtained from *KC* and $KC_{[mod]}$, but not as good as those obtained from K_m and $KC_{[mod]} \times \tau$. However, replacing E_h by $d_{60[m]}$ results in the best *K* estimates of any model tested. Similar to the treatment of the KC model described in equations (1–3), these findings demonstrate how discounting of the cobble framework is necessary to obtain reliable estimates of *K* from electrical-based models.

We find that the reliable prediction of imaginary conductivity (σ'') in the SLP model from a measure of GSD (E_h) also requires discounting for the cobble framework. Using E_h for the full GSD resulted in an overestimation of σ'' for the 10 samples containing a cobble framework, and an underestimation of σ'' for the two sand samples ($\bar{\sigma}_d$ =0.78). This estimation error was substantially reduced when $E_{h[m]}$ was substituted for E_h ($\bar{\sigma}_d$ =0.21). Furthermore, consistent with the findings for the SLP *K* estimation model, the prediction of σ'' is further improved when replacing $E_{h[m]}$ with $d_{60[m]}$ to represent an effective grain diameter ($\bar{\sigma}_d$ =0.21). Similar to *K*, σ'' is insensitive to the surface area contributed by the cobble framework. In the case of *K*, there is not much drag on flow at capillary sides due to cobbles; in the case of σ'', large cobbles do not contribute significantly to S_{por} and represent a negligible fraction of the polarizable grain-fluid interface within the practical frequency range of complex resistivity measurements (0.001–1000 Hz). This equivalent behavior of *K* and σ'' is encouraging with respect to efforts to estimate *K* in coarse unconsolidated conglomeratic

sediments using σ^* measurements. Furthermore this equivalent behavior of K and σ'' with respect to the GSD lends support for the SLP model as a framework for K estimation [*Revil and Florsch*, 2010].

This concept is supported by the estimates obtained from the K prediction model based on a substitution of σ'' for the GSD as presented by *Revil and Florsch* [2010]. Direct application of this equation resulted in a K estimate only slightly worse than that obtained from the Revil and Florsch model when $E_{h[m]}$ was replaced by $d_{eff\ [m]} = d_{60[m]}$. The good prediction from this model is not unexpected if we assume that the interfacial polarization of the cobble framework is negligible within the measured frequency range such that σ'' only senses the polarization of the matrix grains. As already mentioned, the formation factor provides the information on the porosity reduction and tortuosity associated with the presence of the cobble framework. Consequently, equation (16) is well suited for estimating K in samples containing a cobble framework.

Other formulations for the induced polarization response based on polarization mechanisms generated at the interface between large and small pores have been proposed and could have been used to explore linkages with hydraulic conductivity [*Titov et al*., 2002]. In fact, recent work suggests that the pore size (rather than grain size) exerts the primary control on induced polarization [*Revil et al*., 2012]. A benefit of applying the *Revil and Florsch* [2010] model is that the grain size distribution of unconsolidated samples is straightforward to obtain, permitting testing of model predictions as done here. In contrast, pore size distributions require liquid or gas intrusion methods and are not readily available. However, future improvements in the estimation of K from induced polarization measurements will likely result as understanding of linkage between physical properties of porous media and polarization mechanisms continues to improve.

7. Conclusions

Using a set of twelve carefully reconstituted samples, we have shown that the cobble framework of coarse fluvial deposits must be discounted to improve estimates of K using both Kozeny-Carman models and electrical models. In the case of the Kozeny-Carman model, the best estimate of K is achieved when the tortuosity of the matrix capillaries around the cobble framework is included. When the cobble framework is appropriately discounted, the prediction of K using the electrical model of Revil and Florsch, which is based on the formation factor and an effective grain diameter, is surprisingly good given that measured K only varies by a factor of three. The prediction of the imaginary conductivity from the GSD proposed in the Revil and Florsch model also requires discounting for the cobble framework, as the cobble-sized particles polarize at frequencies well below the minimum frequencies used in complex electrical conductivity measurements. Consequently, the imaginary conductivity is directly sensitive to the matrix GSD required to estimate K. The Revil and Florsch parameterization of K prediction based on the formation factor and imaginary conductivity performs well for samples with a cobble framework without modification as the imaginary conductivity directly senses the matrix grain size characteristics, whereas the formation factor captures the porosity reduction and tortuosity resulting from the presence of the cobble framework.

Although variations in the electrical properties of the 12 samples were relatively small, they are well within the resolution of state-of-the-art field-scale electrical imaging systems. Consequently, we argue that there is potential for extracting information on variations in K within coarse conglomeratic deposits at the field scale, despite the narrow range in K that might be encountered in such settings.

Notation

d_{eff}	effective grain diameter providing best approximation to the grain size integral (E_h).
d_0	mean grain diameter as used in the Revil and Florsch model.
d_{10}	grain size at which 10% of the total sample (including the cobble framework) is finer by weight.
d_{50}	grain size at which 50% of the total sample (including the cobble framework) is finer by weight.
d_{60}	grain size at which 60% of the total sample (including the cobble framework) is finer by weight.
d_{90}	grain size at which 90% of the total sample (including the cobble framework) is finer by weight.
$d_{10[m]}$	grain size at which 10% of the matrix portion of sample (diameters less than 0.01 m) is finer by weight.
$d_{50[m]}$	grain size at which 50% of the matrix portion of sample (diameters less than 0.01 m) is finer by weight.

$d_{60[m]}$	grain size at which 60% of the matrix portion of sample (diameters less than 0.01 m) is finer by weight.
D	individual grain diameter.
$f(D)$	probability density distribution of grains of diameter (D) in natural log space.
D^*	diffusion coefficient of ions in the Stern layer.
E_h	integral of the grain size distribution used in the *Revil and Florsch* [2010] model based on the entire sample.
$E_{h[m]}$	integral of the grain size distribution used in the *Revil and Florsch* [2010] model based on the matrix fraction only.
F	electrical formation factor.
g	acceleration due to gravity.
GSD	grain size distribution.
$\varnothing$	total porosity.
$\varnothing_{eff}$	effective porosity representing the interconnected pore space contributing to electrical current flow.
$\varnothing_m$	porosity of the matrix component of the sample.
K	hydraulic conductivity as measured from a traditional Darcy test.
K_{KC}	hydraulic conductivity estimated from the traditional Kozeny-Carman (KC) equation.
$K_{KC[mod]}$	hydraulic conductivity estimated from a modified KC equation after discounting for the cobble framework.
K_m	hydraulic conductivity of the matrix.
m	Archie's cementation exponent.
μ	dynamic viscosity.
η	inverse of grain diameter (D).
ξ	dimensionless normalizing coefficient used in *Revil and Florsch* [2010] model.
ρ_w	fluid density.
S_{por}	interfacial surface area per unit pore volume.
σ^*	complex electrical conductivity.
σ'	real part of the complex electrical conductivity.
σ''	imaginary part of the complex electrical conductivity.
$\lvert\sigma\rvert$	magnitude of the complex conductivity.
σ^*_s	complex surface electrical conductivity.
σ'_s	real part of complex surface electrical conductivity.
σ''_s	imaginary part of complex surface electrical conductivity.
$\bar{\sigma}_d$	average absolute deviation of model predictions from measurements.
Σ^d	specific surface conductivity of the diffuse layer.
Σ^s	specific surface conductivity of the Stern layer.
τ_0	mean time constant of the relaxation distribution.
τ	tortuosity.
σ_{el}	pore fluid conductivity.
V_c	volume fraction of total sample occupied by cobbles.
V_m	volume fraction of total sample occupied by matrix.

Acknowledgments
This material is based upon work supported by the National Science Foundation under grants EAR-0711053 and EAR-0710949. We thank Andre Revil (Colorado School of Mines) for many valuable discussions regarding the content of this manuscript.

References

Archie, G. E. (1942), The electrical resistivity log as an aid in determining some reservoir characteristics, *Trans. Am. Inst. Min. Metall. Pet. Eng.*, *146*, 54–61.

Barrash, W., and M. Cardiff (2013), Hydraulic conductivity distribution from multi-level slug tests and multivariate facies associations in a conglomeratic fluvial aquifer, Boise Hydrogeophysical Research Site, *Tech. Rep. BSU CGISS 13-03*, 71 pp., Boise State Univ., Boise.

Barrash, W., and T. Clemo (2002), Hierarchical geostatistics and multifacies systems: Boise Hydrogeophysical Research Site, Boise, Idaho, *Water Resour. Res.*, *38*(10), 1196, doi:10.1029/2002WR001436.

Barrash, W., and E. C. Reboulet (2004), Significance of porosity for stratigraphy and textural composition in subsurface coarse fluvial deposits, Boise Hydrogeophysical Research Site, *Geol. Soc. Am. Bull.*, *116*(9/10), 1059–1073, doi:10.1130/B25370.1.

Barrash, W., R. Morin, and D. M. Gallegos (1997), Lithologic, hydrologic and petrophysical characterization of a coarse-grained, unconsolidated aquifer, Capital Station site, Boise, Idaho, paper presented at 32nd Symposium on Engineering Geology and Geotechnical Engineering, Boise, Idaho, 26–28 Mar.

Bear, J. (1972), *Dynamics of Fluids in Porous Media*, 764 p., Dover, N. Y.

Binley, A., L. D. Slater, M. Fukes, and G. Cassiani (2005), Relationship between spectral induced polarization and hydraulic properties of saturated and unsaturated sandstone, *Water Resour. Res.*, *41*, W12417, doi:10.1029/2005WR004202.
Boleve, A., A. Crespy, A. Revil, F. Janod, and J. L. Mattiuzzo (2007), Streaming potentials of granular media: Influence of the Dukhin and Reynolds numbers, *J. Geophys. Res.*, *112*, B08204, doi:10.1029/2006JB004673.
Börner, F., and J. Schön (1991), A relation between the quadrature component of electrical conductivity and the specific surface area of sedimentary rocks, *Log Anal.*, *32*, 612–613.
Börner, F. D., J. R. Schopper, and A. Weller (1996), Evaluation of transport and storage properties in the soil and groundwater zone from induced polarization measurements, *Geophys. Prospect.*, *44*(4), 583–601.
Cardiff, M., W. Barrash, M. Thoma, and B. Malama (2011), Information content of slug tests for estimating hydraulic properties in realistic, high-conductivity aquifer scenarios, *J. Hydrol.*, *403*(1–2), 66–82, doi:10.1016/j.jhydrol.2011.03.044.
Cardiff, M., W. Barrash, and P. K. Kitanidis (2013), Hydraulic conductivity imaging from 3D transient hydraulic tomography at several pumping/observation densities, *Water Resour. Res.*, *49*, 7311–7326, doi:10.1002/wrcr.20519.
Carling, P. A., and N. A. Reader (1982), Structure, composition and bulk properties of upland stream gravels, *Earth Surf. Processes Landforms*, *7*, 349–365.
Carman, P. C. (1937), Fluid flow through granular beds, *Trans. Inst. Chem. Eng.*, *15*, 150–166.
Charbeneau, R. J. (2000), *Groundwater Hydraulics and Pollutant Transport*, 593 p., Prentice Hall, Upper Saddle River, N. J.
Church, M. A., D. G. McLean, and J. F. Wolcott (1987), River bed gravels: Sampling and analysis, in *Sediment Transport in Gravel-Bed Rivers*, edited by C. R. Thorne, J. C. Bathurst, and R. D. Hey, pp. 43–88, chap. 3, John Wiley, N. Y.
Clarke, R. H. (1979), Reservoir properties of conglomerates and conglomeratic sandstones, *AAPG Bull.*, *63*(5), 799–809.
Clement, W. P., W. Barrash, and M. D. Knoll (2006), Reflectivity modeling of ground penetrating radar, *Geophysics*, *71*(3), K59–K66, doi:10.1190/1.2194528.
Domenico, P. A., and F. W. Schwartz (1990), *Physical and Chemical Hydrogeology*, 824 p., John Wiley, N. Y.
Freeze, R. A., and J. A. Cherry (1979), *Groundwater*, 604 p., Prentice Hall, Englewood Cliffs, N. J.
Hausrath, E. M., W. Barrash, and E. C. Reboulet (2002), Water sampling and analysis for the Tracer/Time-Lapse Radar Imaging Test at the Boise Hydrogeophysical Research Site, *Tech. Rep. BSU CGISS 02-02*, 86 p., Cent. for Geophys. Invest. of the Shallow Subsurf., Boise State Univ., Boise.
Heinz, J. (2001), Sedimentary geology of glacial and periglacial gravel bodies (SW-Germany): Dynamic stratigraphy and aquifer sedimentology, PhD thesis, 102 p., Univ. of Tubingen, Tubingen, Germany.
Heinz, J., S. Kleineidem, G. Teutsch, and T. Aigner (2003), Heterogeneity patterns of Quaternary glaciofluvial gravel bodies (SW-Germany): Application to hydrogeology, *Sediment. Geol.*, *158*(1–2), 1–23, doi:10.1016/S0037–0738(02)00239-7.
Hu, B. X., M. M. Meerschaert, W. Barrash, D. W. Hyndman, C. He, X. Li, and L. Guo (2009), Examining the influence of heterogeneous porosity fields on conservative solute transport, *J. Contam. Hydrol.*, *108*, 77–88, doi:10.1016/j.jconhyd.2009.06.001.
Jussel, P., F. Stauffer, and T. Dracos (1994), Transport modeling in heterogeneous aquifers: 1. Statistical description and numerical generation, *Water Resour. Res.*, *30*(6), 1803–1817.
Keller, G. V., and F. C. Frischknecht (1966), *Electrical Methods in Geophysical Prospecting*, Pergamon, Oxford, U. K.
Kemna, A., H.-M. Münch, K. Titov, E. Zimmermann, and H. Vereecken (2005), Relation of SIP relaxation time of sands to salinity, grain size and hydraulic conductivity, paper presented at 11th European Meeting of Environmental and Engineering Geophysics.
Klingbeil, R., S. Kleineidam, U. Asprion, T. Aigner, and G. Teutsch (1999), Relating lithofacies to hydrofacies: Outcrop-based hydrogeological characterization of Quaternary gravel deposits, *Sediment. Geol.*, *129*(3–4), 299–310.
Koltermann, C. E., and S. M. Gorelick (1995), Fractional packing model for hydraulic conductivity derived from sediment mixtures, *Water Resour. Res.*, *31*(12), 3283–3297.
Kozeny, J. (1927), Ueber capillary leitung des wassers im boden, *Sitz. Akad. Wiss. Wien*, *136*, 271–306.
Kresic, N. (1997), *Quantitative Solutions in Hydrogeology and Groundwater Modeling*, 461 p., CRC Lewis Publ., N. Y.
Leroy, P., A. Revil, A. Kemna, P. Cosenza, and A. Ghorbani (2008), Spectral induced polarization of water-saturated packs of glass beads, *J. Colloid Interface Sci.*, *321*, 103–117, doi:10.1016/j.jcis.2007.12.031.
Lesmes, D. P., and F. D. Morgan (2001), Dielectric spectroscopy of sedimentary rocks, *J. Geophys. Res.*, *106*(B7), 13,329–13,346, doi:10.1029/2000JB900402.
Lord, M. L., and A. E. Kehew (1987), Sedimentology and paleohydrology of glacial-lake outburst deposits in southeastern Saskatchewan and northwestern North Dakota, *Geol. Soc. Am. Bull.*, *99*, 663–673.
Lunt, I., J. Bridge, and R. Tye (2004), A quantitative, three-dimensional depositional model of gravelly braided rivers, *Sedimentology*, *51*(3), 377–414, doi:10.1111/j.1365-3091.2004.00627.x.
Moret, G. J. M., M. D. Knoll, W. Barrash, and W. P. Clement (2006), Investigating the stratigraphy of an alluvial aquifer using crosswell seismic traveltime tomography, *Geophysics*, *71*(3), B63–B73, doi:10.1190/1.2195487.
Mwenifumbo, C. J., W. Barrash, and M. D. Knoll (2009), Capacitive conductivity logging and electrical stratigraphy in a high-resistivity aquifer, Boise Hydrogeophysical Research Site, *Geophysics*, *74*(3), E125–E133, doi:10.1190/1.3106760.
Oldenborger, G. A., M. D. Knoll, P. S. Routh, and D. J. LaBrecque (2007), Time-lapse ERT monitoring of an injection/withdrawal experiment in a shallow unconfined aquifer, *Geophysics*, *72*(4), F177–F187, doi:10.1190/1.2734365.
Panda, M. N., and L. W. Lake (1994), Estimation of single-phase permeability from parameters of particle size distribution, *AAPG Bull.*, *78*(7), 1028–1039.
Paola, C., and R. Seal (1995), Grain size patchiness as a cause of selective deposition and downstream fining, *Water Resour. Res.*, *31*(5), 1395–1407, doi:10.1029/94WR02975.
Reboulet, E. C., and W. Barrash (2003), Core, grain-size, and porosity data from the Boise Hydrogeophysical Research Site, *Tech. Rep. BSU CGISS 03-02*, 87 p., Cent. for Geophys. Invest. of the Shallow Subsurf., Boise State Univ., Boise, Idaho.
Revil, A. (2012), Spectral induced polarization of shaly sands: Influence of the electrical double layer, *Water Resour. Res.*, *48*, W02517, doi:10.1029/2011WR011260.
Revil, A., and L. M. Cathles (1999), Permeability of shaly sands, *Water Resour. Res.*, *35*(3), 651–662.
Revil, A., and N. Florsch (2010), Determination of permeability from spectral induced polarization data in granular media, *Geophys. J. Int.*, *181*, 1480–1498, doi:10.1111/j.1365-246X.2010.04573.x.
Revil, A., and M. Skold (2011), Salinity dependence of spectral induced polarization in sands and sandstones, *Geophys. J. Int.*, *187*, 813–824, doi:10.1111/j.1365-246X.2011.05181.x.
Revil, A., K. Koch, and K. Holliger (2012), Is it the grain size or the characteristic pore size that controls the induced polarization relaxation time of clean sands and sandstones?, *Water Resour. Res.*, *48*, W05602, doi:10.1029/2011WR011561.

Schwarz, G. (1962), A theory of the low-frequency dielectric dispersion of colloidal particles in electrolyte solution, *J. Phys. Chem.*, *66*(12), 2636–2642.
Scott, J., and R. Barker (2003), Determining pore-throat size in Permo-Triassic sandstones from low-frequency electrical spectroscopy, *Geophys. Res. Lett.*, *30*(9), 1450, doi:10.1029/2003GL016951.
Scott, J., and R. Barker (2005), Characterization of sandstone by electrical spectroscopy for stratigraphical and hydrogeological investigation, *Q. J. Eng. Geol. Hydrogeol.*, *38*, 143–154, doi:10.1144/1470-9326/04-036.
Shih, S.-M., and P. D. Komar (1990), Hydraulic controls of grain-size distributions of bedload gravels in Oak Creek, Oregon, USA, *Sedimentology*, *37*, 367–376.
Slater, L. (2007), Near surface electrical characterization of hydraulic conductivity: From petrophysical properties to aquifer geometries—A review, *Surv. Geophys.*, *28*(2–3), 169–197, doi:10.1007/s10712-007-9022-y.
Slater, L., and D. Glaser (2003), Controls on induced polarization in sandy unconsolidated sediments and application to aquifer characterization, *Geophysics*, *68*(5), 1547–1558, doi:10.1190/1.1620628.
Slater, L., and D. P. Lesmes (2002), Electrical-hydraulic relationships observed for unconsolidated sediments, *Water Resour. Res.*, *38*(10), 1213, doi:10.1029/2001WR001075.
Smith, G. A. (1986), Coarse-grained nonmarine volcaniclastic sediment: Terminology and depositional process, *Geological Society of America Bulletin*, *97*, 1–10.
Sturrock, J. T. (1999), Predictions of hydraulic conductivity using spectral induced polarizations, MS dissertation, Boston College, Chestnut Hill, Mass.
Titov, K., V. Komarov, V. Tarasov, and A. Levitski (2002), Theoretical and experimental study of time domain induced polarization in water-saturated sands, *J. Appl. Geophys.*, *50*, 417–433, doi:10.1016/S0926-9851(02)00168-4.
Todd, S. P. (1989), Stream-driven, high-density gravelly traction carpets: Possible deposits in the Trabeg Conglomerate formation, SW Ireland and some theoretical considerations of their origin, *Sedimentology*, *36*, 513–530.
Tong, M., L. Li, W. Wang, and Y. Jiang (2006a), Determining capillary-pressure curve, pore size distribution and permeability from induced polarization of shaly sand, *Geophysics*, *71*, N33-N40, doi:10.1190/1.2195989.
Tong, M., L. Li, W. Wang, and Y. Jiang (2006b), A time-domain induced-polarization method for estimating permeability in a shaly sand reservoir, *Geophys. Prospect.*, *54*, 623–631, doi:10.1111/j.1365-2478.2006.00568.x.
Vaudelet, P., A. Revil, M. Schmutz, M. Franceschi, and P. Bégassat (2011a), Induced polarization signature of the presence of copper in saturated sands, *Water Resour. Res.*, *47*, W02526, doi:10.1029/2010WR009310.
Vaudelet, P., A. Revil, M. Schmutz, M. Franceschi, and P. Bégassat (2011b), Changes in induced polarization associated with the sorption of sodium, lead, and zinc on silica sands, *J. Colloid Interface Sci.*, *360*, 739–752, doi:10.1016/j.jcis.2011.04.077.
Vinegar, H. J., and M. H. Waxman (1984), Induced polarization of shaly sands, *Geophysics*, *49*(8), 1267–1287.
Zisser, N., A. Kemna, and G. Nover (2010), Relationship between low-frequency electrical properties and hydraulic permeability of low-permeability sandstones, *Geophysics*, *75*(3), E131–E141, doi:10.1190/1.3413260.
Zlotnik, V. A., B. R. Zurbuchen, T. Ptak, and G. Teutsch (2000), Support volume and scale effect in hydraulic conductivity: Experimental aspects, *Spec. Pap. Geol. Soc. Am.*, *348*, 215–231.